indepth

Neurosurgery

Springer Healthcare Education

GUARDING HER TO GROW IN CONFIDENCE

IN TEENS
» No known cosmetic side-effects[1]

IN WOMEN OF CHILDBEARING AGE
» No alteration in menstrual cycle and ovulation[1]

IN ELDERLY WOMEN
» No effect on bone metabolism[1]

START WITH

LEVESAM

Levetiracetam 250/500/750/1000mg Tablets • Levetiracetam Syrup/Injection 100mg/ml

EMPOWER HER

References: 1. Brodie MJ, *et al. Epileptic Disord.* 2003;5(Suppl 1):S65-S72.

COMPOSITION: Each film-coated tablet contains levetiracetam 250 mg / 500 mg / 750 mg /1000 mg. INDICATION: Adjunctive therapy in the treatment of partial onset seizures in adults with epilepsy. DOSAGE AND ADMINISTRATION: (Patients > 16 yrs of age) : Treatment should be initiated with a daily dose of 1000 mg/day, given as twice-daily dosing (500 mg BID), with or without food. Additional dosing increments may be given (1000 mg/day additional every 2 weeks) to a maximum recommended daily dose of 3000 mg, depending upon the clinical response and tolerability. Elderly: Adjust dose in patients with compromised renal function. Renal impairment: Adjust dose according to creatinine clearance. Hepatic impairment: No dose adjustment with mild to moderate hepatic impairment. CONTRAINDICATION: Hypersensitivity to levetiracetam or any ingredient of the formulation. WARNINGS AND PRECAUTIONS: Keep out of reach of children. Central nervous system adverse events, viz. somnolence and fatigue, coordination difficulties, psychotic symptoms and behavioral abnormalities reported to occur most frequently within the first 4 weeks of treatment. Minor hematologic abnormalities also reported. May cause dizziness and somnolence and hence jobs which require extreme alertness should be avoided. Withdrawal of drug: Gradual withdrawal advised. Pregnancy: Should be used only if the potential benefit justifies the potential risk to the fetus. Nursing Mothers: Because of the potential for serious adverse reactions in nursing infants, physician's discretion advised. Drug Interactions: No clinically significant interactions reported. ADVERSE REACTIONS: The most frequently reported adverse reactions are asthenia, headache, infection, pain, anorexia, amnesia, anxiety, ataxia, depression, dizziness, emotional lability, hostility, nervousness, paresthesia, somnolence, vertigo, increased cough, pharyngitis, rhinitis, sinusitis, diplopia. HOW SUPPLIED / STORAGE: Blister pack of 10 tabs. Store in a cool, dry place, protected from light. Please read the full prescribing information available on request with the Medical Services Division, Abbott Healthcare Private Limited, 1st Floor, D Mart Building, Goregaon-Mulund Link Road, Mumbai 400080. Version: 1.06, Dt. 05-04-16

Abridged Prescribing Information: LEVESAM ORAL SOLUTION
COMPOSITION: Each 1 ml contains levetiracetam 100 mg. INDICATION: Adjunctive therapy in the treatment of partial onset seizures in adults in adults and children 4 years of age and older with epilepsy. DOSAGE AND ADMINISTRATION: (Patients > 4 years of age): Treatment should be initiated with a daily dose of 20 mg/day in 2 divided doses(10 mg/kg BID). The daily dose should be increased every 2 weeks by increments of 20 mg/kg to the recommended daily dose of 60 mg/kg, the daily dose may be reduced. Patients with body weight ≤20 kg should be dosed with oral solution. Levetiracetam is given orally with or without food. (Patients >16 yrs of age): Treatment should be initiated with a daily dose of 1000 mg/day, given as twice-daily dosing (500 mg BID), with or without food. Additional dosing increments may be given (1000 mg/day additional every 2 weeks) to a maximum recommended daily dose of 3000 mg. CONTRAINDICATION: Hypersensitivity to levetiracetam or any ingredient of the formulation. WARNINGS AND PRECAUTIONS: Keep out of reach of children. Central nervous system adverse events, viz. somnolence and fatigue, coordination difficulties, psychotic symptoms and behavioral abnormalities reported to occur most frequently within the first 4 weeks of treatment. Minor hematologic abnormalities also reported. May cause dizziness and somnolence and hence jobs which require extreme alertness should be avoided. Withdrawal of drug: Gradual withdrawal advised. Pregnancy: Should be used only if the potential benefit justifies the potential risk to the fetus. Nursing Mothers: Because of the potential for serious adverse reactions in nursing infants, physician's discretion advised. Drug Interactions: No clinically significant interactions reported. ADVERSE REACTIONS: The adverse events most frequently reported with the use of Levetiracetam in combination with other AEDs in pediatric patients were somnolence, accidental injury, hostility, nervousness and asthenia. The most frequently reported adverse events associated with the use of levetiracetam in combination with other AEDs in adults were somnolence, asthenia, infection and dizziness. Of the most frequently reported adverse events in adults were asthenia, somnolence and dizziness is reported to occur predominantly during the first 4 weeks of treatment with levetiracetam. HOW SUPPLIED / STORAGE: Syrup is available in bottle pack of 100 ml. Store in a cool, dry place, protected from light. Keep out of reach of children.

Please read the full prescribing information before usage.
For additional information, please contact Medical Services Division,
Abbott Healthcare Pvt. Ltd.
Floor 18, Godrej BKC, Plot No. C-68, Near MCA Club, Bandra-Kurla
Complex, Bandra East, Mumbai 400051. www.abbott.co.in
Copyright 2018 Abbott. All rights reserved.
Version : 1.0, Dt. 19.06.2014

INDLVM185007a 28 NOV 2018

Abbott

indepth

Neurosurgery

Springer Healthcare Education

December 2018

Springer Healthcare

This edition is created in India for free distribution in India.
This edition is published by Springer Nature India Private Limited.
Registered Office: 7th Floor, Vijaya Building, 17, Barakhamba Road, New Delhi 110 001, India.
91 (0) 11 4575 5888
www.springerhealthcare.com

Part of the Springer Nature group

Contents

Step by step procedure to view the online contents and video(s):

1. **Go to** http://collections.medengine.com/neurology/in-depth-neurosurgery/ **or scan QR code.**

2. Web page of the issue will be opened.

3. You can read the PDF and view the video(s) online. Both can be downloaded also.

Neuroimaging in Epilepsy

Anuradha Singh, Priyanka Sabharwal, Timothy Shepherd

Computed Axial Tomography

Computed tomography (CT) is widely available and used in emergency rooms. With multiple detector helical CT, high spatial resolution can be obtained in all dimensions allowing 3D reconstructions and operator selected multiplanar reformats in any plane. CT may be the only option in patients who cannot obtain MRI due to contraindications such as patients with pacemakers, defibrillators, specific metal prostheses (e.g., cochlear implants), ferromagnetic aneurysm clips, metallic foreign bodies within eyes, and shrapnel or bullets located near vascular structures. There may be other barriers in obtaining a conventional MRI in unstable or uncooperative patients, or patients with significant claustrophobia or morbid obesity. CT scans provide better details about bony structures and can easily detect hemorrhages, calcifications, strokes after 24 h, and large tumors. However, CT may fail to recognize commonly encountered lesions in patients with epilepsy such as hippocampal atrophy, hippocampal sclerosis, cortical dysplasias, or low-grade gliomas (LGG).

Magnetic Resonance Imaging (MRI)

Magnetic resonance imaging is a noninvasive test, which does not cause exposure to ionizing radiations and is considered safe across all age groups. It possesses excellent spatial resolution

A. Singh (✉)
Department of Neurology, Bellevue Hospital Center, 462, 1st Avenue and 27th Street, NBV 7W11, New York, NY 10016, USA
e-mail: anuradha.singh@bellevue.nychhc.org; anuradha.singh@nyumc.org

P. Sabharwal
Department of Neurology, NYU Langone Medical Center, 223 East 34th Street, New York, NY 10016, USA
e-mail: priyanka.sabharwal@nyumc.org

T. Shephard
Department of Radiology, New York University Langone Medical Center, 660 First Ave., 2nd Floor, New York, NY 10016, USA
e-mail: timothy.shepherd@nyumc.org

down to millimeters. MRI scanners with higher magnetic strengths (3-, 4-, or 7-Tesla) have proliferated over the past decade. The typical MRI epilepsy protocol includes multiplanar diffusion, T2-weighted, FLAIR, gradient echo, or susceptibility-weighted images of the brain. This protocol is supplemented with a 3D volumetric T1-weighted acquisition and oblique coronal plane FLAIR and T2-weighted images orthogonal to the long axis of the temporal lobes. Gadolinium administration may have utility in certain patient populations with seizures or when there is clinical suspicion for infectious, inflammatory, or neoplastic etiologies.

The presence or absence of lesion(s) and their location on brain MRI helps identify patients who may be good surgical candidates for lesionectomy, corticectomy, topectomy, corpus callosotomy, or hemispherectomy. For example, patients with medically refractory seizures and hippocampal sclerosis should be evaluated for either standard anterior temporal lobe resection or selective amygdalohippocampectomy. A lesionectomy of a cavernoma with or without corticectomy is a reasonable option if anti-seizure medications are not effective in controlling seizures. A more aggressive surgical approach, such as a functional hemispherectomy, may be warranted in patients with Sturge-Weber syndrome, Rasmussen's encephalitis, large porencephalic cyst due to previous traumatic or ischemic insult, hemimegalencephaly, or Dyke–Davidoff–Masson syndrome (congenital or acquired). Neuroimaging may have a direct influence on therapeutic options that neurologists offer to their patients; e.g., a scan supporting a diagnosis of tuberous sclerosis (TS) in an infant with infantile spasms may justify the use of vigabatrin or m-TOR inhibitors over adrenocorticotropic hormone (ACTH). Not all structural lesions are epileptogenic; therefore, it is prudent to correlate incidental findings on MRI with clinical history, seizure semiology, and EEG data. Some of the commonly encountered lesions in patients with epilepsy are described below.

Mesial temporal sclerosis: Temporal lobe epilepsy (TLE) is the most common form of focal epilepsy. Mesial TLE is more prevalent than neocortical epilepsy and often intractable to anti-seizure medications. The most common identifiable lesion on MRI brain is mesial temporal sclerosis (MTS; Fig. 1). In patients with TLE, subtle anatomic features of the medial temporal lobes and pathologies such as MTS or incomplete hippocampal inversion (Fig. 2) are best appreciated in an oblique coronal plane. This orientation is orthogonal to the long axis of the temporal lobe and reduces volume averaging problems for the thin laminar appearance of the hippocampus. Oblique coronal temporal high-resolution T2-weighted and FLAIR are the best sequences to diagnose MTS. This entity is characterized by (1) hippocampal atrophy, (2) increased T2 signal, and (3) abnormal morphology or loss of internal architecture of hippocampus. In 10% of the cases, MTS can be bilateral (Fig. 3). Secondary findings may include dilatation of the temporal horn of the lateral ventricle, loss of gray–white matter differentiation in the temporal lobe or decreased white matter in the adjacent temporal lobe (e.g., collateral eminence and temporal stem). There can be atrophy of the ipsilateral fornix and mammillary body (Fig. 4). High-resolution 3D T1WI are also useful when performing hippocampal volumetric analyses. However, paracentral lesions are more evident on axial sequences. Figure 5 shows a less common case of temporal lobe seizures from a temporal lobe encephalocele involving the subjacent sphenoid wing.
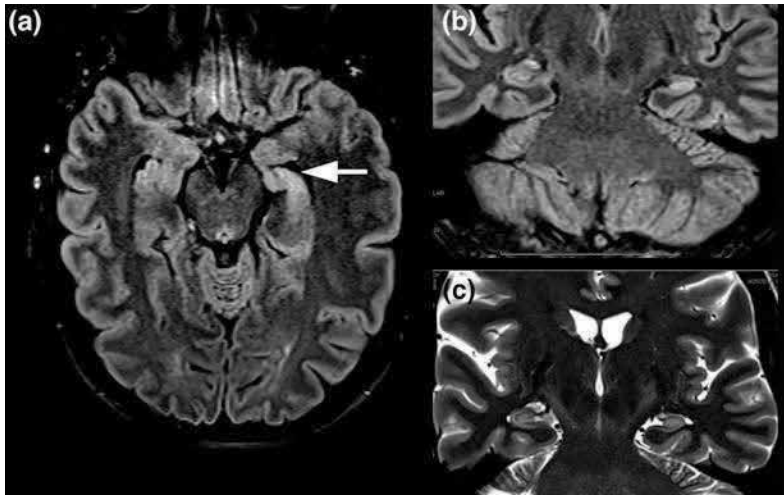
Fig. 1: Axial FLAIR (**a**) demonstrates enlargement of the left lateral ventricle temporal horn and the left hippocampus is relatively smaller and hyperintense compared to the contralateral side. Note that the lateral aspect of the left hippocampal body is abnormally smooth, and hippocampal head digitations are reduced (*arrow*). Companion coronal FLAIR (**b**) and T2-weighted MRI (**c**) demonstrate volume loss, hyperintensity, and subtle laminar blurring. These are classic MRI findings for left hippocampal sclerosis. If the amygdala also is involved, this can be classified as left mesial temporal sclerosis.
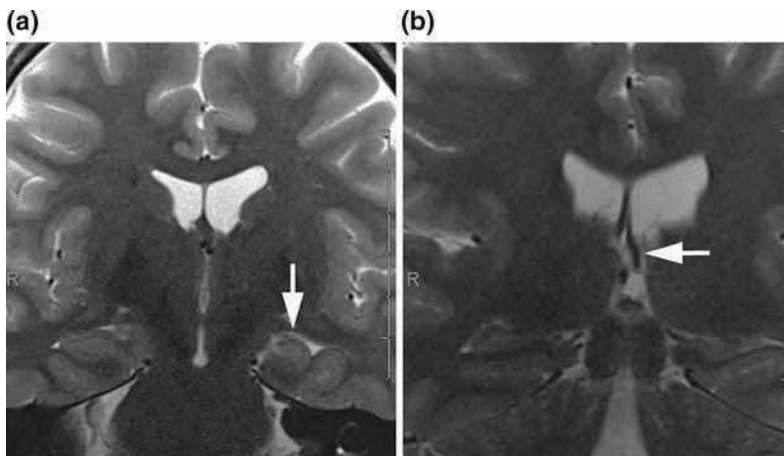

**Fig. 2:** Coronal T2-weighted images demonstrating globular left hippocampus (*arrow*, panel **a**) more vertical left collateral sulcus and low-lying left body of the fornix (*arrow*, panel **b**) consistent with incomplete hippocampal inversion (IHI). This patient also had left hippocampal sclerosis, but it remains controversial whether IHI predisposes to sclerosis or is just an incidental association.

Fig. 3: Coronal FLAIR (**a**), T2-weighted (**b**) and 3D T1-weighted demonstrate bilateral hippocampal body hyperintensity, laminar blurring, and volume loss, respectively. Findings are consistent with bilateral hippocampal sclerosis.
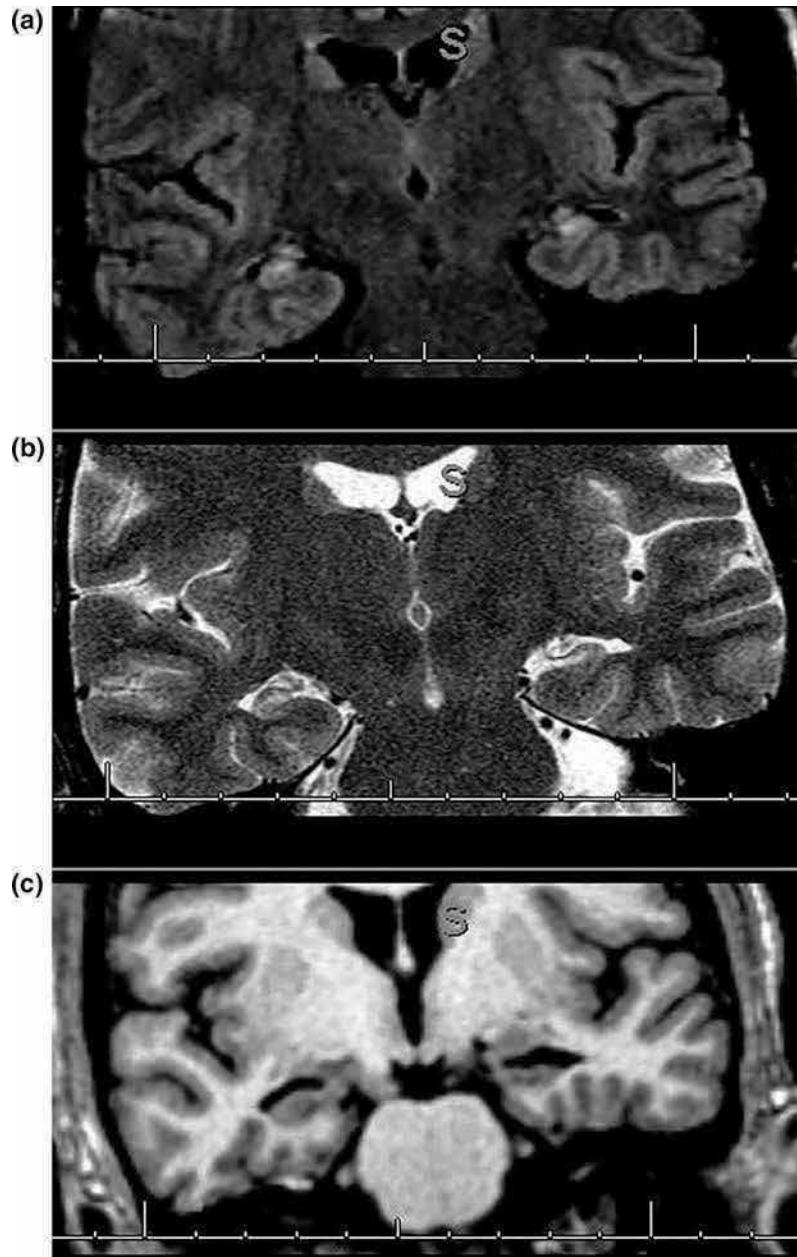
Neuronal migrational disorders: Heterotopias are neuronal migrational disorders (NMDs) where gray matter gets arrested as neurons migrate from periventricular regions toward pia during embryonic stages. High-resolution 3D T1-weighted volumetric imaging provides superior gray–white contrast that is critical to identify subtle cortical malformations in patients with epilepsy (Fig. 6). Higher magnetic strengths (3- or 7-Tesla) can detect very subtle cortical dysplasias.
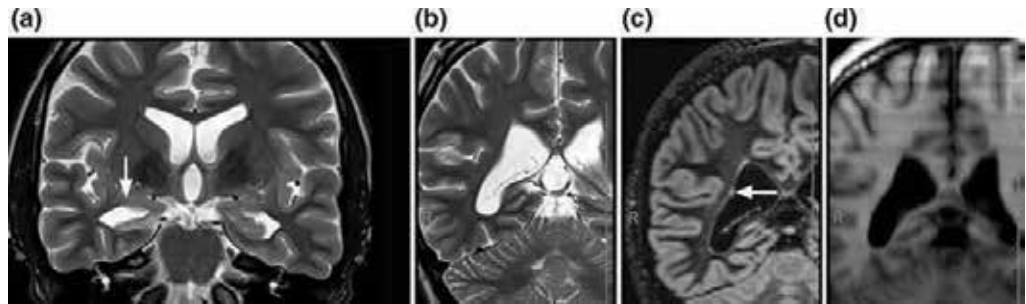
Fig. 4: Oblique coronal T2 demonstrates obvious volume loss and laminar blurring of the right hippocampal head (*arrow*, panel **a**) consistent with right hippocampal sclerosis and right fornix atrophy (**b**). There is a small gray matter heterotopia in the lateral wall of the right lateral ventricle, best seen on the coronal double-inversion recovery image (*arrow*, panel **c**) compared to companion T2 and T1-weighted MRI (**b** and **d**).
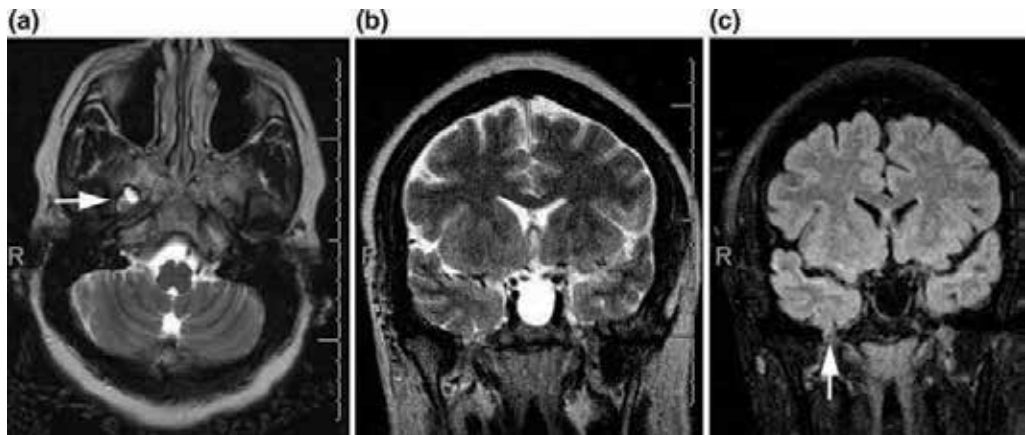

Fig. 5: Axial and coronal T2-weighted MRI, and coronal FLAIR demonstrate a small encephalocele that involves a focal portion of the fusiform gyrus cortex extending into the right foramen ovale (*arrows*). The MRI abnormality is not always associated with seizures, but should be considered suspicious. In this case, the finding was concordant with semiology and EEG.

Heterotopias can either be focal, nodular, or multifocal (as in TS) or preferentially involve one hemisphere as in hemimegalencephaly. Subcortical band heterotopias (SBH) are typically periventricular, bilateral nodular collections of gray matter with relatively smooth margins, which gives the appearance of a double cortex. Pachygyria is abnormal tissue in the right location with abnormal sulcation and gyration of the mantle which is typically > 8 mm thick (Fig. 7a). Polymicrogyria (PMG) is either two- or four-layered cortex, which is less than 5–7 mm (Fig. 7b). PMG is commonly associated with hypoxic-ischemic injury, or prenatal cytomegalovirus (CMV) infection.

Focal cortical dysplasias (FCDs) are classified into three categories (types I, II, and III) and further divided into various subtypes (Table 1). In a fully myelinated brain, FCD type I may be characterized by subtle blurring of the gray–white junction with typically normal cortical thickness, moderately increased white matter signal hyperintensities on T2/FLAIR images and
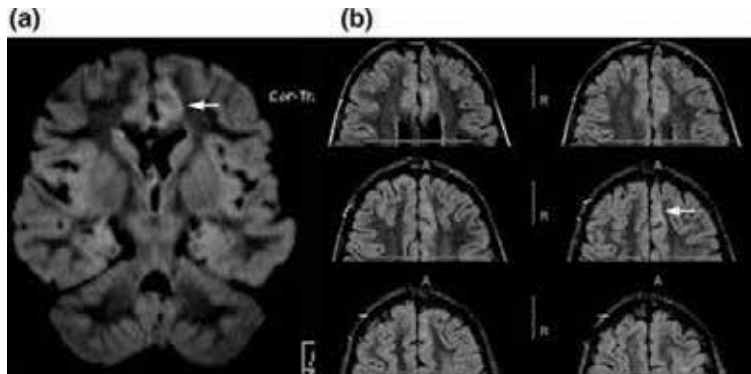
Fig. 6: Coronal FLAIR MRI (**a**) and serial axial FLAIR MRI of the frontal lobes (**b**) demonstrating subtle *gray–white* blurring and FLAIR hyperintensity in the left anterior cingulate gyrus and adjacent left medial frontal gyrus (*arrows*) from a pathologically proven cortical dysplasia.
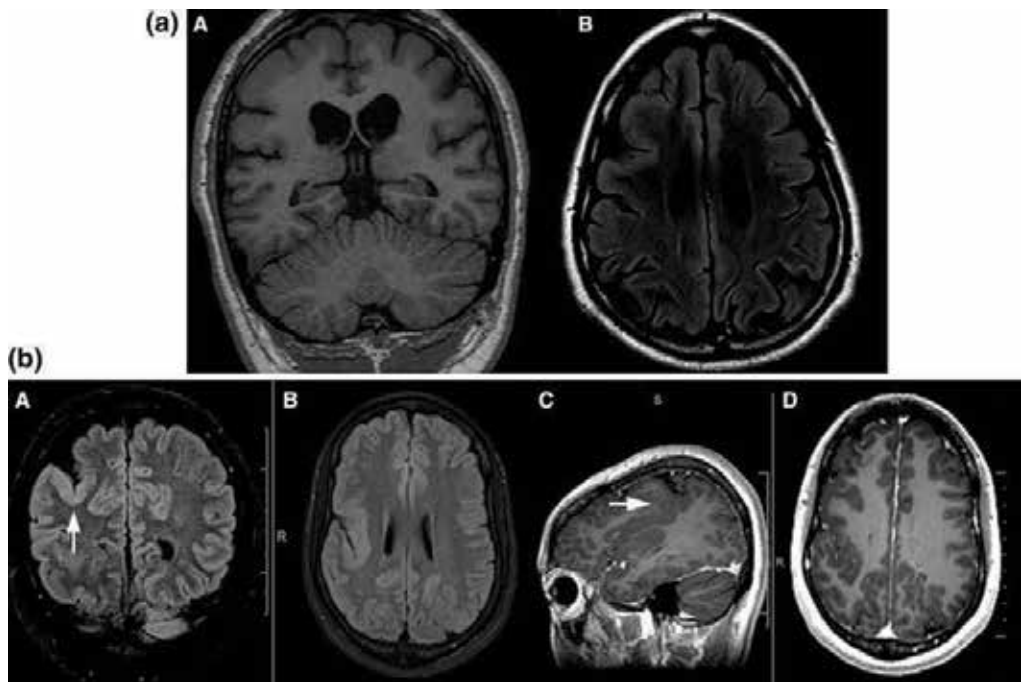
Fig. 7: (**a**) Coronal 3D T1-weighted (**A**) and axial FLAIR MRI (**B**) demonstrate broad, simplified gyri with relatively shallow sulci in the bifrontal regions compared to the temporal and parietal regions consistent with pachygyria. (**b**) Coronal and axial FLAIR (**A** and **B**), sagittal, and axial post-contrast 3D T1 (**C** and **D**) MRI show abnormal cortex that appears thickened extending from the posterior right Sylvian fissure (*arrow*). The fissure is lengthened with a vertical orientation toward the vertex (*arrow*, panel **C**). Findings consistent with unilateral polymicrogyria.

Table 1: Classification of focal cortical dysplasias.

Types	Features
Type I	Ia: abnormal vertical alignment of neurons Ib: abnormal horizontal alignment Ic: horizontal and vertical malalignment
Type II	IIa: dysmorphic neurons without balloon cells IIb: dysmorphic neurons with balloon cells
Type III	IIIa: mesial temporal sclerosis IIIb: glioneural tumors e.g., ganglioglioma, DNET IIIc: vascular malformations (CCMs, AVMs, telangiectasias, and meningioangiomatosis) IIId: prenatal or perinatal ischemic injury, TBI, and scars due to inflammatory or infectious lesions

decreased signal intensity on T1-weighted images. FCD Type IIA cortical dysplasias are characterized by marked blurring of the gray–white junction on T1 and T2-FLAIR images due to hypomyelination or dysmyelination of the subcortical white matter with or without cortical thickening. Here, the increased white matter signal changes on T2, WI, and FLAIR images frequently tapers toward the ventricles (aka the "*transmantle sign*") which marks the involvement of radial glial neuronal bands. This radiological feature differentiates FCD from low-grade tumors. Type II lesions are more commonly seen outside the temporal lobe with predilection for the frontal lobes. Type III FCD is typically associated with another principal lesion such as hippocampal sclerosis, tumor, a vascular malformation, or other acquired pathology during early life.

Other important NMDs include lissencephaly, which is characterized by smooth brain surface and abnormal gyration, which varies between agyria and pachygyria. Lissencephaly with posteriorly predominantly gyral abnormalities is caused by mutation in LIS1 gene (Fig. 8). Anteriorly predominant lissencephaly in heterozygous males and subcortical band heterotopia (SBH) in heterozygous females are caused by mutations of the XLIS (double cortex gene on chromosome X). Schizencephaly is another rare form of MCD which is characterized by the presence of a transcortical cleft that can extend from ventricles to the pia with open or fused lips, and often polymicrogyria is seen on the lips of the schizencephaly (Fig. 9). Hemimegalencephaly is the unilateral hamartomatous excessive growth of all or part of one cerebral hemisphere at different phases of embryologic development. MRI in these cases reveals an enlarged hemisphere with increased white matter volume, cortical thickening, agyria, pachygyria, polymicrogyria or lissencephaly, and blurring of the gray–white matter junction. Often, a large, ipsilateral irregularly shaped ventricle may be seen.

Brain tumors: Approximately 20–40% of the adults with primary brain tumors experience one seizure prior to the tumor diagnosis, and another 20–45% will suffer from seizures during the course of the illness [1]. This incidence rate varies depending on the tumor type, the grade of the tumor, and its location. Seizures are more common in slow growing tumors such as meningiomas, gangliogliomas (GGs), dysembryoplastic neuroepithelial tumors (DNETs), or diffuse low-grade tumors such as Grade II astrocytomas, oligodendrogliomas, and oligoastrocytomas (Table 2). Typically, the low-grade tumors do not enhance on Gd-administration. The most common location is temporal lobe, followed by the parietal, frontal, and occipital lobes. Gangliogliomas typically present with temporal lobe epilepsy, presumably due to the temporal lobes being a favored
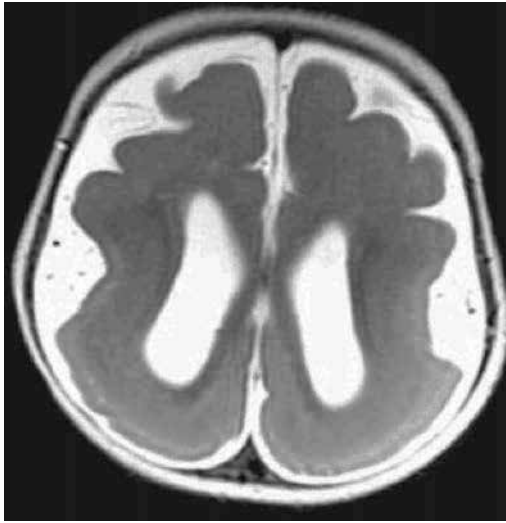
Fig. 8: MRI brain axial T2-weighted image shows lissencephaly agyria and smooth brain. Especially posteriorly in a patient with LIS1 mutation.

Fig. 9: CT brain axial image shows a cleft in the left hemisphere consistent with schizencephaly.

location (Fig. 10). Gangliogliomas are closely related to gangliocytomas, which contain essentially only mature neural ganglion cells, and ganglioneurocytoma, which in addition have small mature neoplastic neurons. On MRI, these tumors may show cystic changes or calcifications.

Dysembryoplastic neuroepithelial tumors are cortically based benign neoplastic cortical malformations, which may show subcortical extension in approximately 30% of tumors giving them a triangular appearance (Fig. 11). These tumors appear as well-defined lobulated, and solid tumors that are hyperintense on T2WI and may erode the overlying calvarial bone or show micro-cystic changes. The most common location is temporal (60%) followed by temporal lobes (30%). Meningiomas are the most common extra-axial tumors of the central nervous system. They
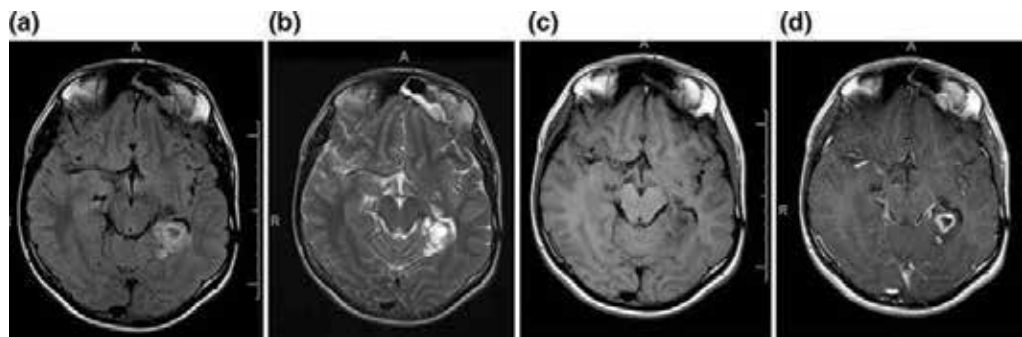

Fig. 10: Axial FLAIR (**a**), T2-weighted (**b**), pre-contrast (**c**), and post-contrast T1-weighted MRI (**d**) demonstrating solid and cystic mass in the left posteromedial temporal lobe with focal areas of contrast enhancement most consistent with ganglioglioma. CT also often demonstrates focal calcification.

Table 2: Common epilepsy associated tumors.

Tumors	Radiological features
Meningioma	Isointense on T1 and T2; homogeneous enhancement with Gd, extra-axial, dural tail, and CSF cleft sign
Ganglioglioma	Cyst with enhancing mural nodule/solid; calcifications in ~50%
Dysembryoplastic neuroepithelial tumors (DNET)	Bubbly cystic appearance with small cysts within the tumor that are hyperintense on T2WI, wedge shaped mass which expands the affected gyri and point toward the ventricle, swollen gyrus, may be associated with focal cortical dysplasia
Pleomorphic xanthoastrocytoma (PXA)	Supratentorial cyst with enhancing mural nodule which abuts the peripheral meninges, peritumoral edema, mild meningeal enhancement
Oligodendroglioma	Hypointense on T1, hyperintense on T2, calcification seen as areas of blooming, 50% enhance heterogeneously, minimal peritumoral edema
Hypothalamic hamartomas	Nonenhancing non-neoplastic congenital gray matter heterotopia in the region of tuber cinereum of the hypothalamus which can be sessile or pedunculated
Subependymal giant cell astrocytomas (SEGA)	Heterogeneous mass near the Foramen of Monro, usually >1 cm; hypo or isointense on T1 and hyperintense on T2, marked enhancement; other findings of tuberous sclerosis such as cortical tubers and subependymal nodules, "transmantle sign" in some tubers; nodular, ill-defined, cystic and band-like lesions seen in the white matter and radial bands
Glioblastoma multiforme (GBM)	Hypo or isointense on T1, hyperintense on T2, vasogenic edema, susceptibility artifact on T2 from intratumoral lesions due to hemorrhage or rarely calcification, "butterfly glioma" when bilateral and cross the corpus callosum, necrosis may be present, peripheral or irregular nodular enhancement; no diffusion restriction but lower ADC than low-grade tumors
Metastases	Hypointense on T1 (except melanomas can be hyperintense), hyperintense on T2 and FLAIR, intense enhancement (ring-enhancing, punctate or uniform), often multiple lesions present at diagnosis, vasogenic edema out of proportion to the size of the lesion, hemorrhage, and necrosis may be seen

are nonglial neoplasms that originate from the arachnoid cap cells of the meninges and have characteristic imaging findings, although there are many variants (Fig. 12). GBMs are aggressive malignant tumors that are associated with significant vasogenic edema and heterogeneous enhancement. The overall incidence of seizures in Grade IV glioblastoma multiforme (GBM) patients, without considering the location, has been reported between 25 and 50% at presentation and another 20–30% during the course of the disease [2]. Metastatic lesions tend to have a smaller risk for seizures, one exception being metastatic melanoma.

Perfusion-weighted imaging is a useful tool, which involves several image acquisitions during the first pass of a bolus of contrast agent. This method allows the radiologist to determine the relative cerebral blood volume (rCBV). In general, the underlying principle is the greater the rCBV, the higher the grade of tumor. Lack of notable flow indicates a nonneoplastic etiology with abnormal signal intensity, such as demyelination. Of note, mixed oligodendrogliomas can have low rCBV. Besides the prognostic information it provides, perfusion-weighted imaging can increase the yield of brain biopsy and help in differentiating recurrent neoplasm from radiation necrosis. On perfusion MRI, GBMs typically show increased regional blood flow (Fig. 13).
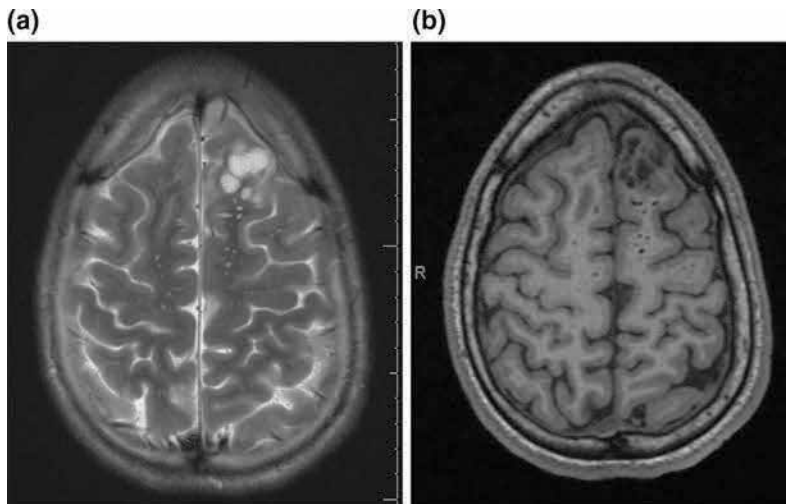
Fig. 11: Axial T2- and T1-weighted MRI (**a** and **b**) demonstrate bubbly T2 bright lesion in the left superior frontal gyrus with minimal mass effect that does not enhance (contrast not shown). In a patient with seizures, these findings are most consistent with dysembryoplastic neuroepithelial tumor (DNET).
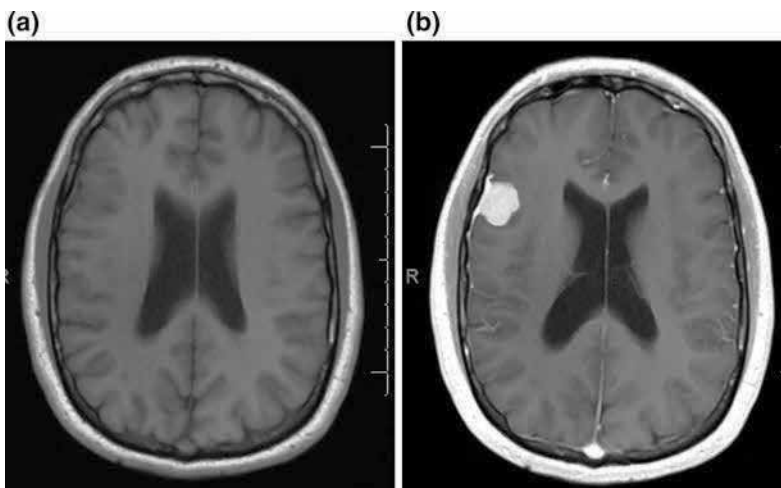

Fig. 12: Axial pre-contrast (**a**) and post-contrast T1-weighted MRI (**b**) demonstrate an extra-axial mass overlying the right frontal operculum that is isointense to gray matter and shows homogeneous enhancement with dural tail consistent with meningioma.

Another interesting but rare kind of focal congenital tumor is hypothalamic hamartoma (HH). These tumors are typically associated with ictal spells of laughter without mirth or gelastic seizures (Fig. 14). HH are composed of cytologically normal, small, and large neurons, which are organized in poorly demarcated clusters of variable size and density. These tumors are categorized by the Delalande classifications I–IV. Type I has a horizontal orientation and may be lateralized on one side; Type II has a vertical orientation and an intraventricular location; Type III is a combination of types I and II; Type IV is a giant hamartoma.
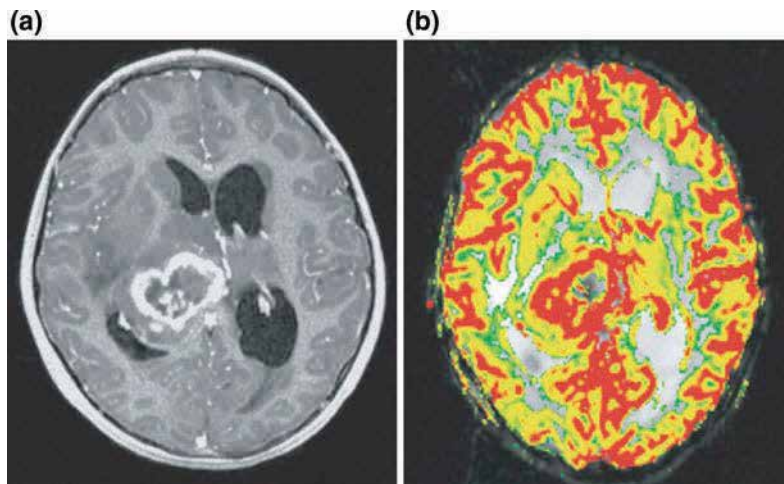
Fig. 13: MRI brain post-Gd T1-weighted image (**a**) showing ring enhancement in the right thalamus and *deep gray* structures with associated mass effect, midline shift, and obstructive hydrocephalus. Pathology was consistent with glioblastoma multiforme. Perfusion MRI (**b**) shows increased regional cerebral blood flow at the tumor margins.
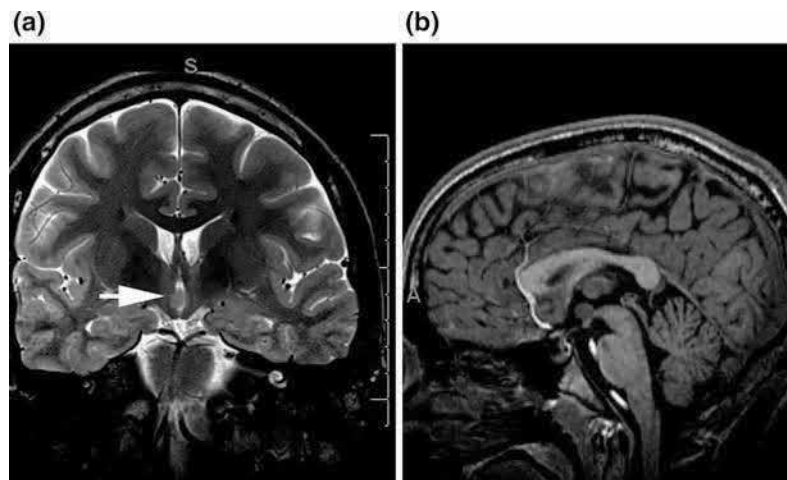

Fig. 14: Coronal T2-weighted (**a**) and sagittal T1-weighted MRI (**b**) demonstrating ectopic gray matter along the wall of the 3rd ventricle (*arrow*) in adolescent patient with gelastic seizures. Findings support diagnosis of hypothalamic hamartoma.

Vascular malformations: Vascular malformations can be either high flow or low flow. High flow malformations include arteriovenous malformations (AVMs), which can be parenchymal, dural, or mixed. In contrast, low flow vascular malformations are cerebral cavernous malformations (CCMs), developmental venous anomaly (DVA), or mixed vascular malformations (Fig. 15). CCMs have a unique "popcorn" appearance with hemorrhages of different ages. They may be bright on CT due to pooling of blood within the cavernoma. The most characteristic feature is

blood products of different ages with an area of hyperintensity representing methemoglobin surrounded by a hypointense ring of hemosiderin on T2W MRI. Gradient echo (GRE) sequences are useful to detect CCMs and may show low or minimal enhancement on Gd. MRI brain is superior to CT scan to look for the nidus of an AVM which is hyperdense compared to adjacent brain (Fig. 16). It is easier to appreciate fast flow voids on T2WI due to fast flow and enlarged draining veins may be seen. Phase contrast MR angiography can help subtract the hematoma components in patients who present with acute hemorrhage into an AVM. CTA can demonstrate feeding arteries, nidus, and draining veins visible, which resembles a "bag of worm" appearance. The exact anatomy of feeding vessels and draining veins is often difficult to delineate, and thus angiography remains necessary. Digital subtraction angiography (DSA) remains the gold standard in delineating the location and number of feeding vessels supplying the central nidus and the pattern of venous drainage (superficial or deep). The susceptibility-weighted images (SWI) are particularly sensitive to iron content in the brain, both in cortical layers and in blood vessels and identify hemosiderin in CCMs, old infarcts or old contusions.

Infectious/inflammatory disorders: A common etiology for seizures in all age groups, both in the developing and developed world, includes infections of the nervous system. A wide variety of pathogens including viral, bacterial, fungal, parasitic, and other opportunistic pathogens can cause CNS disease in humans. Though gold standard of diagnosis remains either biopsy or CSF analysis, neuroimaging can aid in rapid diagnosis by helping identify typical lesion patterns. While it is outside the scope of this chapter to comprehensively discuss CNS infections, we have attempted to list typical radiology findings with common CNS infections associated with epilepsy in Table 3. More recent MRI techniques, such as DWI and MRS also aid in diagnosis by providing additional information, which is discussed in relevant sections in this chapter. Briefly, restricted diffusion helps in differentiation of progenitor abscesses from ring-enhancing lesions of other etiology. Also, the presence of lactate and cytosolic amino acids and the absence of choline on MRS are seen in the cases of pyogenic abscesses. Autoimmune encephalitis can also be associated with seizures. Figure 17 illustrates an example of progressive volume loss and denudation of the overlying cortex Rasmussen's syndrome is one kind of autoimmune encephalitis associated with
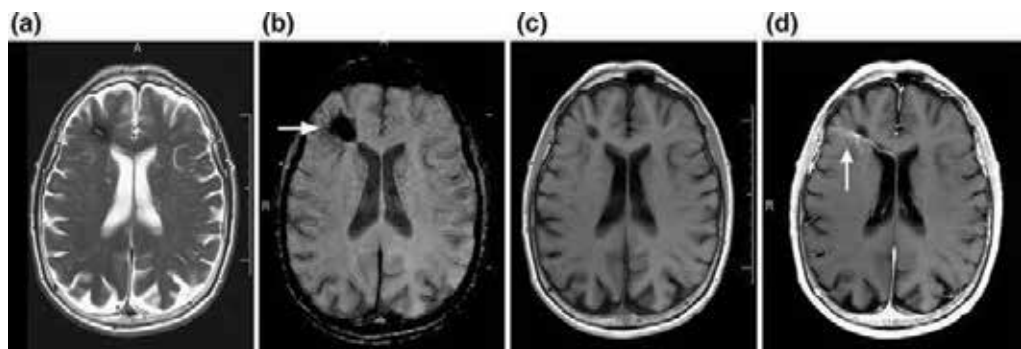

Fig. 15: Axial T2-weighted and axial susceptibility-weighted MRI (**a** and **b**) demonstrate a popcorn-like T2 bright lesion with surrounding hypointense susceptibility (*arrow*). Pre- and post-contrast axial MRI (**c** and **d**) demonstrate associated developmental venous anomaly (*arrow*) strongly supporting diagnosis of cavernoma.
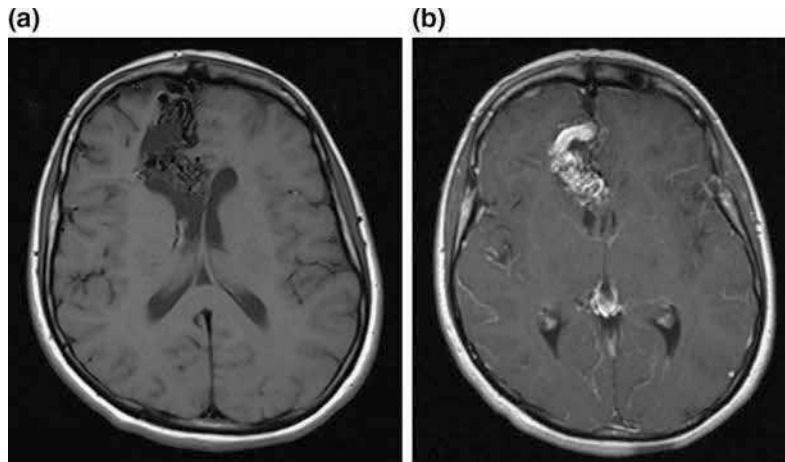
Fig. 16: MRI brain axial T1-weighted image (**a**) shows right mesial frontal arteriovenous malformation. Post-Gd T1-weighted (**b**) reveals enlarged draining vein.
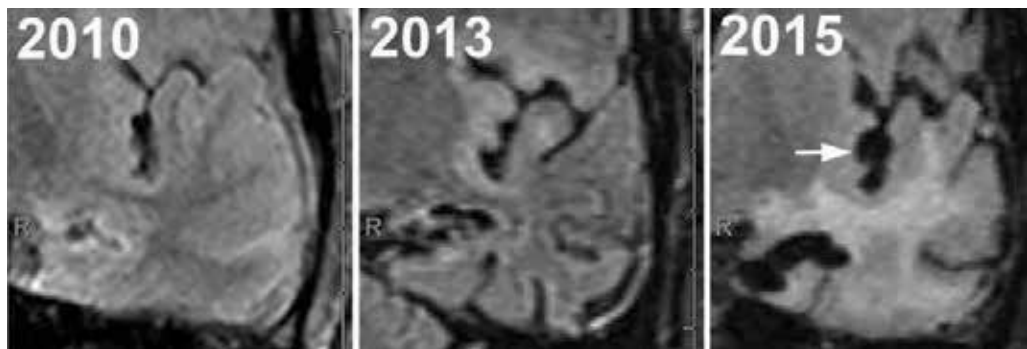

Fig. 17: Serial coronal FLAIR images of the left temporal lobe in an adult patient with autoimmune encephalitis. Between 2010 and 2015, there was progressive volume loss and denudation of the overlying cortex (*arrow*). Similar focal lobar volume loss can happen in Rasmussen encephalitis.

intractable unilateral seizures, progressive hemiparesis or weakness on one side, and intellectual dysfunction.

Neurocutaneous Syndromes (Phacomatoses): These are a group of inherited disorders characterized by hamartomas and neoplasms throughout the body along with involvement of the nervous system and skin. The neuroradiological features of common phacomatoses, namely, tuberous sclerosis (TS), neurofibromatosis (NF1 and NF2), and Sturge Weber syndrome (SWS) are summarized in Table 4.

Figure 18 illustrates a few salient neuroradiological features of TS and SWS in patients with medically refractory seizures.

Trauma: Traumatic brain injury (TBI), especially severe closed skull injury and penetrating dural injury have been well documented to cause post-traumatic epilepsy [3]. Patients with prolonged loss of consciousness, post-traumatic amnesia, or hemorrhage in the brain (subarachnoid

Table 3: Radiological features of common infections.

Infections	Radiological features
Brain abscess	Ring of isodense or hyperdense tissue with central hypoattenuation on CT. MRI classically shows T1 hypointense, T2/FLAIR hyperintense, diffusion restricted lesion. The four stages of an abscess with imaging findings are listed below: * Early cerebritis—Poorly marginated cortical or subcortical hypodensity with mass effect with little or no enhancement * Late cerebritis—irregular rim enhancing lesion with hypodense center, better defined than early cerebritis * Early capsule—well-defined rim enhancing mass; an outer hypodense and inner hyperdense rim (double rim sign) classically * Late capsule—rim enhancing lesion with thickened capsule and diminished hypodense central cavity
CNS tuberculosis	Can be leptomeningeal, pachymeningeal, or intracranial (tuberculomas) * Leptomeningeal—intense heterogenous basal enhancement * Pachymeningeal—intense enhancement of thickened meninges * Intracranial: T1 isointense with central hyperintensity (possible caseation), T2 isointense with central hyperintensity (possible gliosis), ring-enhancing
Herpes simplex encephalitis	Preferential involvement of mesial temporal lobes. If hemorrhagic, blooming on GRE/SWI
Japanese encephalitis	Predominant involvement of deep gray matter, especially bilateral thalami (though may be asymmetric) with sparing of cortices
Rabies encephalitis	In classic cases, increased T2 signal in affected parts with predilection for the gray matter especially basal ganglia, thalami, hypothalami, brain stem, limbic system, and spinal cord as well as the frontal and parietal lobes
Neurocysticercosis	Findings are based on location (parenchymal or in sub-arachnoid-intraventricular space; which appears grape-like (racemose) cystic, often associated with ventriculitis) or stage of infection (as below). * Vesicular—T1 hyperintense scolex ±, Cyst with dot sign (parasitic cyst with eccentric scolex), no or faint enhancement * Colloidal vesicular—T1 hyperintense with surrounding edema, scolex with eccentric focus of enhancement * Granular nodular—edema decreases, cyst retracts, enhancement persists but less marked from prior stage * Nodular calcified—end-stage quiescent, no edema, no enhancement
Toxoplasmosis	Multiple lesions, T1 isointense or hypointense and T2 isointense to hyperintense, with predilection for basal ganglia and corticomedullary junction that often show ring or nodular enhancement. Increased lipid lactate peak on MRS is characteristic.
Schistosomiasis	Rare, seen either as intracerebral and intracerebellar hematomas or nonspecific granulomatous lesions (hypodense on CT and T1-hypointense and T2-isointense on MRI) due to a response of the host to the ova
Toxocariasis	Multiple cortical, sub-cortical, or white matter lesions that are hypodense on CT, hyperintense on T2-weighted MRI images, and homogeneously enhancing
Cryptococcosis	Leptomeningeal involvement, "soap bubble" appearance with pseudocysts—common in mid brain and basal ganglia with parenchymal cryptococcomas. Also, tendency to spread along peri-vascular spaces with dilated perivascular spaces

Table 4: Neuroradiological findings in common phacomatoses.

| Phacomatoses	Neuroradiological findings
NF1 (peripheral)	Optic glioma, peripheral or cranial nerve sheath tumors, macrocephaly, sphenoid wing dysplasia, scoliosis, astrocytomas
NF2 (central)	Vestibular schwannomas, meningiomas, schwannomas/neurilemmomas of the dorsal roots of the spinal cord
TS	Cortical tubers (calcifications, cysts, or fibrosis may be seen in tubers), subependymal nodules (SENs), SENs near the foramen may enhance on Gd and transform into a SEGA → serial MRIs may show progressive growth, papilledema, and obstructive hydrocephalus; white matter heterotopias, arachnoid cyst, aneurysms
SWS	Leptomeningeal angiomatoses, calcification of gyri in form of rail-road shape, cerebral atrophy, venous, or arterial infarcts
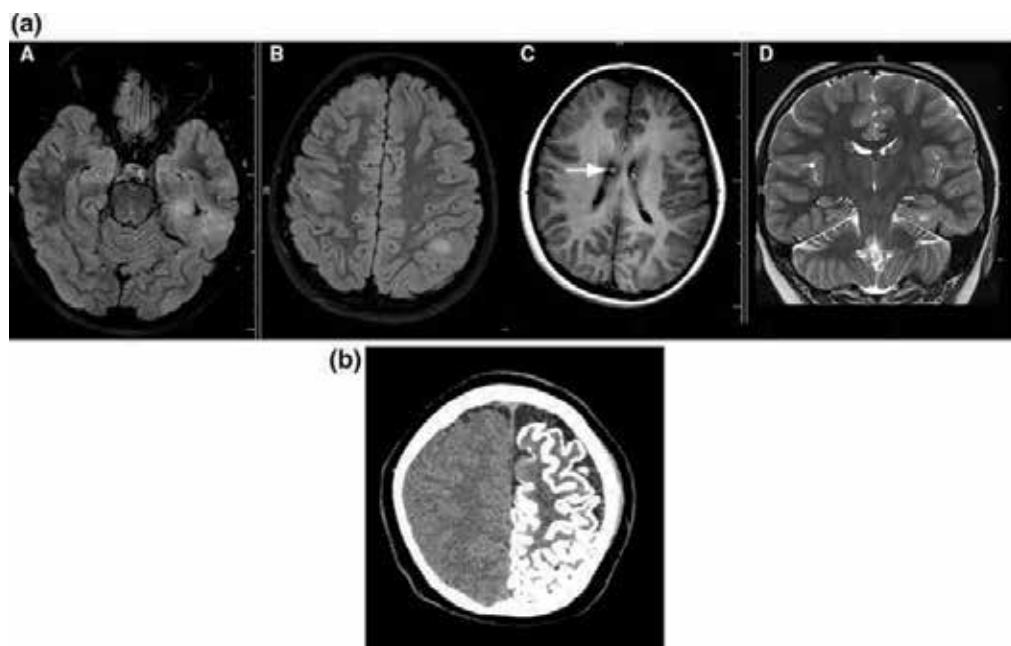
Fig. 18: Axial FLAIR (**a**, **b**) demonstrates focal T2 hyperintense masses in the cortex and subcortical white matter of the basal left temporal lobe and left inferior parietal lobule consistent with tubers. Axial pre-contrast T1 and coronal T2-weighted MRI demonstrate multiple ependymal nodules along the bilateral caudothalamic grooves. These lesions demonstrate subtle T1 hyperintensity (*arrow*) attributed to calcification that can be seen on CT (*not shown*). Video EEG suggested the adjacent tubers in the posterior basal left temporal lobe were responsible for the majority of seizures in this patient with tuberous sclerosis. Axial CT slice (**c**) demonstrating cortical tram-track calcification throughout most of the left cerebral hemisphere consistent with pial angiomatosis. There is a volume loss, but with relative sparing of the left frontal operculum. Findings are consistent with Sturge-Weber syndrome.

Table 5: Radiographic findings in patients with TBI.

Pathology	Comments
Gliding contusions	Due to sagittal angular acceleration with stretching and tearing of parasagittal veins
Hemorrhages	Scalp hematoma, subdural, epidural, subarachnoid, intraparenchymal, ventricular with or without mass effect
Diffuse axonal injury (DAI)	Areas affected are parasagittal regions of the frontal lobes, periventricular areas in temporal lobes, near internal and external capsules, gray–white matter junctions, dorsolateral quadrants of the rostral brainstem, and cerebellum. GRE and SWI show small regions of susceptibility artifacts

hemorrhage, subdural, epidural, intraparenchymal, and intraventricular) are at a higher risk of developing immediate (onset within 24 h), early (onset within a week), or late-onset epilepsy. The findings on imaging vary from contusions, with or without diffuse axonal injury (DAI), or hemorrhages in different locations (Table 5). T2WI and the FLAIR images are sensitive to edema in the brain, while GRE and SWI are very sensitive to microhemorrhages. Figure 19 shows temporal encephalomalacia as a result of TBI. SWI and DWI are the best sequences to detect DAI. Tong *et al*. group showed that number of hemorrhagic DAI lesions seen on SWI was six times greater than that on conventional T2-weighted 2D GRE imaging and the volume of hemorrhage was approximately twofold greater.

Positron Emission Tomography (PET)

Positron emission tomography is a noninvasive, diagnostic imaging technique for measuring the metabolic activity of cells in the human body. PET studies characterize genotype–phenotype
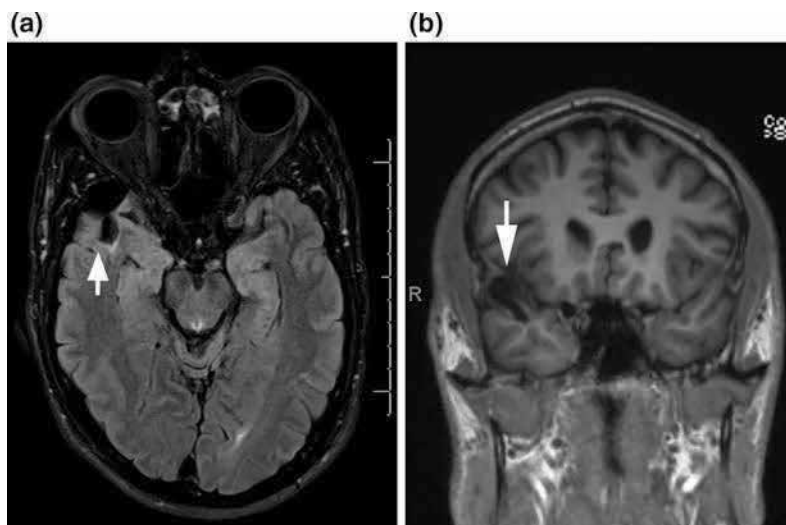

Fig. 19: Axial FLAIR (**a**) and coronal 3D T1-weighted MRI (**b**) demonstrating subtle encephalomalacia in the anterior right superior temporal gyrus (*arrows*) attributed to remote trauma in a patient with seizures and history of high-speed motor vehicle accident.

Table 6: Common ligands used during PET scans.

Types of PET	Techniques used
FDG	Glucose metabolism
H_2O	Cerebral blood flow
[^{11}C] Carfentanil	Binds to mu-opiate receptors
[^{11}C] Doxepin	Binds to histamine H1 receptors
α [^{11}C] methyl-L-Tryptophan	Measures tryptophan metabolism by serotonin and kynurenine pathways
[^{11}C] Flumazenil	Measures tryptophan metabolism by serotonin and kynurenine pathways

interactions because this technique directly measures neurometabolic changes and receptor binding. PET produces images of the body by detecting the radiation emitted from radioactive substances. These substances are injected into the body and are usually tagged with a radioactive atom (^{11}C, ^{18}Fl, ^{15}O or ^{13}N) that has short decay time (Table 6). The radioactivity localizes in the appropriate areas of the body and is detected by the PET scanner.

Different colors and/or degrees of brightness on a PET image represent different levels of tissue or organ function. For example, as healthy tissue uses glucose for energy, it accumulates some of the tagged glucose, which shows up on PET images. However, epileptogenic tissue during interictal phases utilizes less glucose than healthy normal tissue, and thus, it appears less bright than normal tissue on the PET images (Fig. 20). ^{18}F FDG-PET is particularly helpful in identifying subtle FCDs. FDG is useful for tumor grading because most high-grade tumors, such as high-grade gliomas, medulloblastoma, and primary central nervous system lymphoma, have high concentrations and activity of glucose transporters (GLUTs). Most low-grade tumors have lower concentrations of GLUTs and can usually be distinguished from high-grade gliomas by the lower FDG uptake on PET [4]. FDG-PET is a useful tool in distinguishing post-radiation necrosis from tumor progression, both in high-grade gliomas and brain metastases. In general, recurrent tumor is FDG avid, and radiation necrosis is not FDG avid.
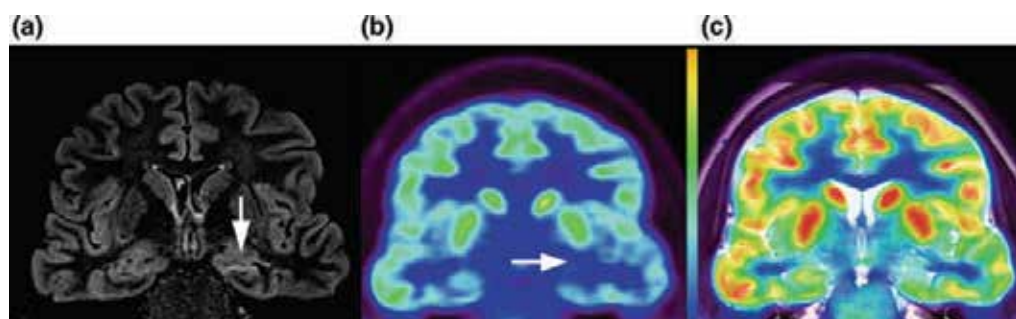

Fig. 20: Simultaneous PET-MRI technology in a temporal lobe epilepsy patient. Coronal FLAIR demonstrates volume loss and hyperintensity in the left hippocampal head (*arrow*, panel **a**). Coronal FDG demonstrates hypometabolism that involves both medial and lateral left temporal lobe (*arrow*, panel **b**). Blended images combining MRI and FDG data can also be obtained to assist visual detection of abnormalities (here, FLAIR with color FDG map superimposed).

Subtraction Ictal SPECT Co-Registered to MRI (SISCOM)

Subtraction ictal SPECT co-registered to MRI is a novel neuroimaging technique that couples MR images with nuclear medicine single-photon emission computed tomography (SPECT) scans to identify areas of increased perfusion with respect to regional cerebral flow (rCBF). It is commonly used as a tool in pre-surgical evaluation to localize the seizure focus in both pediatric and adult patients with refractory epilepsy [5]. Technically, radio tracer injections (typically Tc-99 m) are administered during an ictal event that allows computation of variations in rCBF between ictal and inter-ictal states. Studies by multiple groups have validated SISCOM as a valuable tool that offers improved localization of seizure focus by visualization of the region of hyperperfusion and thus higher neuronal activity (40–86%). Further, SISCOM findings serve as a guide for further intracranial monitoring, electrode placement, and in determining the extent of surgical resection, which in turn offers a higher probability of post-surgical seizure freedom [6–8]. Occasionally, incongruous findings have been reported between intracranial vEEG and SISCOM in post-surgical patients [5]. These likely reflect an altered blood flow pattern in these patients rather than the actual seizure onset zone. However, SISCOM still exists as a valuable tool in pre-surgical planning in both identification of the ictal zone and guiding surgical resection. For the clinician, though, it is essential to remember that the complete workup must be tailored to each individual patient.

Magnetoencephalogram (MEG)

Magnetoencephalogram measures small electrical currents arising inside the neurons of the brain, which produce very weak magnetic fields in the range of femto and pica Tesla. Patient wears a helmet containing an array of 100+ sensitive magnetic field measurement devices. The measurement devices are called superconducting quantum interference devices (SQUIDS). MEG has a high resolution in both space (2–3 mm) and time (<1 ms). The skull and the tissue surrounding the brain affect the magnetic fields measured by MEG much less than they affect the electrical
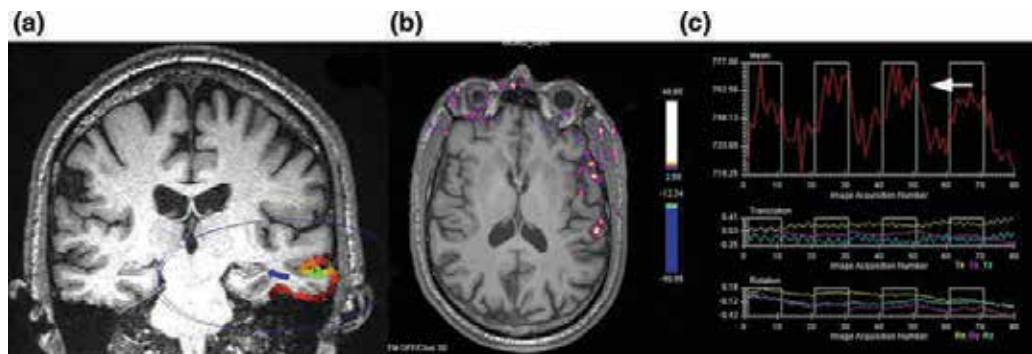

Fig. 21: Advanced imaging workup in patient with MRI-negative left temporal lobe epilepsy. Coronal MPRAGE with interictal MEG dipole cluster in the left middle temporal gyrus (*blue arrow*, panel **a**) was concordant with semiology and EEG. Task-based functional MRI of the patient performing word generation task demonstrates left language dominance (**b**). A region-of-interest of BOLD signal in the planum temporale (presumably Wernicke's area) demonstrated a strong correlation with performance of the task (*arrow*, panel **c**).

impulses measured by electroencephalogram. MEG is usually performed with simultaneous EEG. For magnet source imaging (MSI), information from MEG and MRI is coregistered to form magnetic source localization images that provide detailed structural–functional information of the brain. MSI helps in characterization and localization of epileptiform activity and pre-operative mapping of brain areas supporting sensory, motor, and language function (Fig. 21). MSI is complimentary to PET, fMRI, and EEG as it provides unique information on the spatiotemporal dynamics of brain activity.

Diffusion-Weighted Imaging (DWI)

Diffusion-weighted imaging adds spatially encoding magnetic gradients to the standard MRI sequence to make the image sensitive to the translational motion of water molecules. In the absence of T2 weighting, the "bright regions" represent decreased water diffusion, and "dark regions" represent increased water diffusion. Hence an acute stroke with cytotoxic edema and slow water diffusion will appear very bright. However, a T2-bright tissue, such as edema or gliosis from a late subacute or chronic infarct, also can appear bright on a diffusion trace image (this is called "T2 shine through"). In apparent diffusion coefficient (ADC) maps calculated from the diffusion-weighted images, the intensity of pixels is more directly proportional to extent diffusion, and the T2 weighting is removed from the data. A bright signal on DWI and dark signal on ADC supports the evidence of cytotoxic edema seen with infarctions (Table 7). A focus of increased signal intensity on DWI with a normal ADC signal suggests vasogenic edema and referred to as "T2 shine through."

Diffusion Tensor Imaging (DTI)

Diffusion tensor imaging is based on the basic principle that the diffusion of water molecules in the brain is restricted by intracellular and extracellular membranes, particularly myelin. The image intensities are inversely related to the relative mobility of water molecules in tissue and the direction of motion. Anisotropy is a measure of the orientation-dependent water diffusion within an image voxel, e.g., CSF has a fractional anisotropy of near zero, whereas highly coherent white matter has a fractional anisotropy near 1. The diffusion data can also be given color codes based on principal direction of diffusion, and the intensity of color is proportional to the fractional

Table 7: DWI and ADC characteristics in different disorders.

Pathology	DWI	ADC	Cause
Stroke	High	Low	Cytotoxic edema
Solid tumor	Variable	Variable	Depends on the cellularity
Arachnoid cyst	Low	High	CSF signal intensity
Herpes encephalitis	High	Low	Cytotoxic edema
Abscess	High in the center	Low	Dense pus
Acute diffuse axonal injury	High	Low	White matter shearing

anisotropy. The transverse axis (*x*-axis) is represented by red color; the green color depicts anterior posterior (*y* axis), and blue is designated to superior inferior (*z*-axis). DTI tractography then uses fractional anisotropy and the principal orientation of diffusion with the voxel to characterize the coherent white matter bundle 3D orientations with the brain and spinal cord. Thus, tractography allows accurate diagnosis of even subtle congenital and acquired lesions that might disrupt the axonal organization.

Practical applications of DTI and tractography in epilepsy include precise delineation of white matter tracts in the brain, especially in identification of eloquent white matter tracts, such as the arcuate fasciculus adjacent to neoplasms or epileptogenic regions [9, 10]. Another area where tractography has significant implications is in mapping of optic radiations during pre-surgical planning of anterior temporal lobe resection procedures. Here, pre-operative tractography can demonstrate the anterior extent of Meyer's loop, which is variable between people and cannot be visualized on traditional MRI studies. Thus, one can predict the extent of visual field defects that might happen post-surgery. DTI has relatively poor spatial resolution and is less sensitive to injury at crossing fibers and close to gray–white matter junction [11, 12].

Magnetic Resonance Spectroscopy (MRS)

In the field of epilepsy, MRS acts as a valuable tool by complementing MRI. While conventional MRI is very helpful in studying anatomy, MRS offers a noninvasive means to determine the biochemical and metabolic characteristics of the tissue of interest. Though both are based on similar principles, MRS uses signal from protons to estimate the concentration of metabolites, chiefly N-acetyl aspartate (NAA), choline (Cho), creatine (Cr), and lactate in brain tissue. 1H spectroscopy, most widely used, is useful for assessment of markers of neuronal loss such as NAA, products of anaerobic metabolism such as lactic acid, and direct measures of primary excitatory and inhibitory neurotransmitters. 31P spectroscopy is directed toward the characterization of the bio energetic status of the tissue of interest phosphocreatine (PCr), adenosine triphosphate (ATP), and phosphoinositol (Pi).

Applications of MRS in epilepsy imaging are widespread. In patients with hippocampal sclerosis, the MRS shows evidence of neuronal dysfunction such as decreased NAA and decreased NAA/Cho and NAA/Cr ratios and decreased myo inositol (MI) in ipsilateral temporal lobe and increased lipid and lactate soon after a seizure [13]. Conventionally, MRS has been used in characterization and differentiation of masses that appear equivocal on MRI. MRS can help differentiate between dysplastic versus neoplastic masses, recurrent brain neoplasm versus radiation injury, or between an abscess versus a tumor [14]. Further, MRS has also been used to screen for inborn errors of metabolism such as Canavan's disease and creatine deficiency. There is a typically decreased NAA/Cr ratio in patients with dysplastic cortex as in hemimegalencephaly. Interestingly, multiple studies have now validated MRS as a tool in identifying the seizure focus, thus making it useful in the evaluation of both focal and generalized epilepsy. Work by numerous groups has shown specific metabolic abnormalities that are confined to the seizure zone [15, 16]. Inter-ictal changes include increased inorganic phosphate (Pi), increased pH, and decreased

phosphomonoesters, a decreased PCr/Pi ratio together with a decrease in NAA (reduction of 22% ipsilateral to seizure focus). Also, an increase in lactic acid is usually seen post-ictally. While MRS has been reported to have localizing value by numerous groups (65–96% chances of lateralization in TLE by proton MRS and 65–75% value in TLE by phosphorus MRS), research is still ongoing to determine the value of MRS in localization of the epileptogenic focus.

Functional MRI (F-MRI)

Functional MRI is a noninvasive imaging technique that has grown in popularity over the past two decades. Its role has been increasingly recognized in clinical practice to lateralize language and motor functions. The intracarotid sodium amobarbital angiographic procedure (the "Wada") and intraoperative cortical stimulation mapping procedures are still the clinical gold standards to localize the epileptogenic zone and map the functional areas of the brain. However, these mapping techniques have their own limitations due to after discharges and seizures produced by stimulation. The spatial resolution of fMRI is great, but the temporal resolution is suboptimal for dissecting out the different functional areas of the brain that are related to a particular task.

References

1. Glantz MJ, Cole BF, Forsyth PA, *et al*. Practice parameter: anticonvulsant prophylaxis in patients with newly diagnosed brain tumors. Report of the Quality Standards Subcommittee of the American Academy of Neurology. Neurology. 2000;54(10):1886–93.
2. Moots PL, Maciunas RJ, Eisert DR, Parker RA, Laporte K, Abou-Khalil B. The course of seizure disorders in patients with malignant gliomas. Arch Neurol. 1995;52(7):717–24.
3. Annegers JF, Hauser WA, Coan SP, Rocca WA. A population-based study of seizures after traumatic brain injuries. N Engl J Med. 1998;338(1):20–4.
4. Horky LL, Treves ST. PET and SPECT in brain tumors and epilepsy. Neurosurg Clin N Am 2011;22(2):169–84.
5. So EL. Integration of EEG, MRI, and SPECT in localizing the seizure focus for epilepsy surgery. Epilepsia. 2000;41(Suppl 3):S48–54.
6. Bianchin MM, Wichert-Ana L, Velasco TR, Martins AP, Sakamoto AC. Imaging epilepsy with SISCOM. Nat Rev Neurol. 2011;7(4):1–2.
7. Ahnlide JA, Rosén I, Lindén-Mickelsson Tech P, Källén K. Does SISCOM contribute to favorable seizure outcome after epilepsy surgery? Epilepsia. 2007;48(3):579–88.
8. Van Paesschen W. Ictal SPECT. Epilepsia. 2004;45(Suppl 4):35–40.
9. Yogarajah M, Duncan JS. Diffusion-based magnetic resonance imaging and tractography in epilepsy. Epilepsia. 2008;49(2):189–200.
10. Luat AF, Chugani HT. Molecular and diffusion tensor imaging of epileptic networks. Epilepsia. 2008;49(Suppl 3):15–22.
11. Duncan JS. Imaging the Brain's highways – diffusion tensor imaging in epilepsy. Epilepsy Currents. 2008;8(4):85–9.
12. Gross DW. Diffusion tensor imaging in temporal lobe epilepsy. Epilepsia. 2011;52(Suppl 4):32–4.
13. Caruso PA, Johnson J, Thibert R, Rapalino O, Rincon S, Ratai EM. The use of magnetic resonance spectroscopy in the evaluation of epilepsy. Neuroimaging Clin N Am. 2013;23(3):407–24.
14. Kuzniecky R. Clinical applications of MR spectroscopy in epilepsy. Neuroimaging Clin N Am. 2004;14(3):507–16.
15. Laxer KD. Clinical applications of magnetic resonance spectroscopy. Epilepsia. 1997;38(Suppl 4):S13–7.
16. Garcia PA, Laxer KD, Ng T. Application of spectroscopic imaging in epilepsy. Magn Reson Imaging. 1995;13(8):1181–5.

Laminectomy

Zachary A. Medress, Yi-Ren Chen, Ian Connolly, John Ratliff, Atman Desai

Introduction

Spinal stenosis is the most common indication for surgery in the lumbar spine [1]. A minimally invasive approach through a tubular retractor provides direct surgical access to decompress the central canal and lateral recess in patients with evidence of central stenosis due to broad based disc bulges, ligamentum flavum hypertrophy, and facet arthropathy. Benefits of a minimally invasive laminectomy include smaller incision, less muscular disruption and pain, reduced blood loss and rate of blood transfusion, reduced rate of blood transfusion, preservation of components of the midline tension band including interspinous ligaments, spinous process, supraspinous ligament.

Indications

Patients suited for a MIS laminectomy include those that present with neurogenic claudication from central canal stenosis and/or lumbar radiculopathy from lateral recess stenosis. Unilateral or bilateral lateral recess stenosis from ligamentum flavum hypertrophy, facet arthropathy should be visualized on MRI at a level that corresponds with the patient's symptoms in the absence of spondylolisthesis, deformity, or evidence of motion on lumbar flexion-extension X-rays.

Contraindications

Patients who present with back pain or mechanical instability are unlikely to derive benefit from a minimally invasive laminectomy. Preoperative imaging that demonstrates deformity or high grade spondylolisthesis is a contraindication. Some surgeons believe that minimally invasive laminectomy may be performed in patients with non-mobile grade I spondylolisthesis without

Z.A. Medress, Y.-R. Chen, I. Connolly, J. Ratliff (✉), A. Desai
Department of Neurosurgery, Stanford University, Stanford, CA, USA
e-mail: zmedress@stanford.edu; trinxile@stanford.edu; jratliff@stanford.edu; atman@stanford.edu

causing worsening instability. However, MIS laminectomy should be avoided in mobile or high grade spondylolisthesis as it may worsen instability. Prior surgery at the same level is a relative contraindication to an MIS approach given the presence of scar tissue and unpredictable tissue plans that may be difficult to navigate through a small operative corridor, though not an absolute contraindication.

Surgical Technique

The patient is positioned prone on a Wilson frame. All bony prominences should be adequately padded, and the abdomen should be allowed to hang freely in order to reduce venous hypertension and resultant epidural bleeding. The Wilson frame should be optimally positioned in order to increase intralaminar space. Using fluoroscopy, the appropriate level is identified and a skin incision is made 1–2 cm off midline. Bovie electrocautery is used to dissect to the level of the lumbodorsal fascia, which is sharply incised. The dilator is docked on the inferior lamina in a sweeping fashion in order to dissect away soft tissue. Lateral fluoroscopy is again used to confirm correct docking position on the inferior lamina of the superjacent level, and sequential dilators are used to sweep away soft tissue and introduce the tubular working channel. Soft tissue is remove from the lamina using bovie electrocautery and pituitary rongeurs. The laminectomy is performed with a high speed drill and kerrison rongeurs starting at the inferior lamina. The ligamentum flavum is dissected, undercut, and removed using a nerve hook, angled curettes, and kerrison rongeurs. The dura should be visibly decompressed, and meticulous hemostasis should be obtained in the epidural gutter using Floseal (Baxter, Deerfield, IL), Gelfoam (Pfizer, New York, NY), and cottonoids. Once adequate decompression has been obtained, the tubular retractor is slowly removed, and hemostasis is obtained using bipolar cautery in the muscular and subcutaneous layers through the tubular retractor given that areas of bleeding may be difficult to find after the retractor has been removed.

Of note, bilateral decompression can be accomplished from one side, docking only from one side and extending the bony removal to the deep part of the spinous process and contralateral lamina, achieving bilateral access in that fashion. Anterior-posterior fluoroscopy can be utilized when needed to confirm laterality (Figs. 1 and 2).

Pearls and Pitfalls

Downward pressure should be maintained on the dilators at all time during docking to avoid unintentional migration of the working channel. Ideally, the inferior edge of the lamina should be centered in the operative field in order to serve as an anatomic landmark prior to drilling.

Complications

Potential complications from MIS laminectomy include wrong level surgery, durotomy, CSF leak, inadequate decompression, hematoma, nerve root injury, wound infection, creation of mechanical
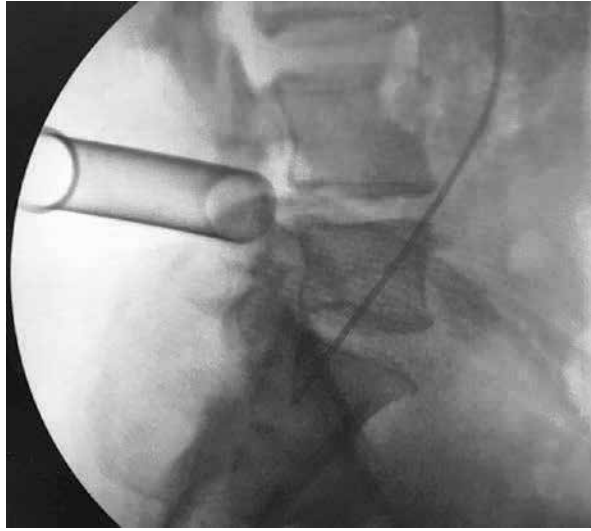
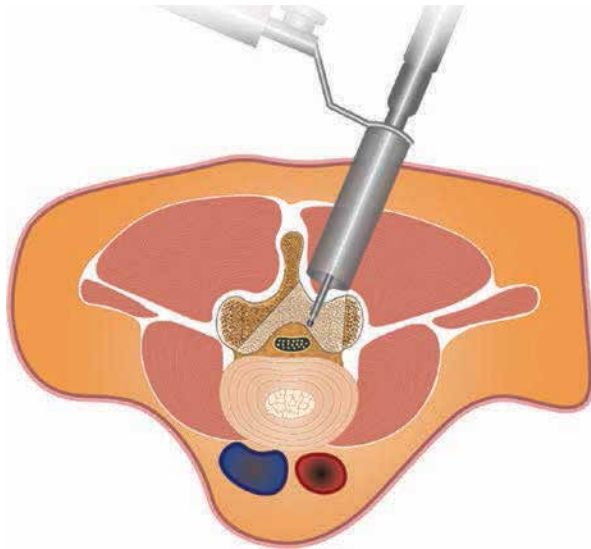**Fig. 1:** Example docking for a L4–5 decompression.

Fig. 2: Example approach to bilateral decompression, MIS.

instability from overly aggressive bony removal. In cases where a durotomy has occurred, an MIS approach provides the benefit of involving less dead space and tissue disruption. In such cases, a primary dural repair may be achieved and a dural sealant may be used to reinforce a primary repair. In cases of durotomy, a water-tight fascial closure is mandatory, and may be aided by the use of a hyper-curved needle such as UR-6 (Ethicon, Somerville, NJ). Conversion to open may be necessary in some cases if significant CSF leak is encountered.

Literature Review

Minimally invasive laminectomy remains a bread and butter procedure for the treatment of lumbar spinal stenosis. In the 1970s, Caspar and Yasargil introduced microsurgical techniques to the treatment of lumbar disc herniation [2]. In experienced hands, durotomy occurs in less than 5% of cases using a minimally invasive approach, and nearly 90% of patients are discharged within 24 h of the operation [3]. Meta-analysis of open versus MIS laminectomy demonstrate that MIS laminectomy is associated with increased satisfaction, lower blood loss, lower pain scores, and similar complication rates including CSF leak and infection, though MIS operations were significantly longer than open approaches by 11 min [4]. Bilateral decompression through a unilateral tubular MIS approach can be safely and efficiently achieved without introducing clinically significant instability [5]. Given the small working corridor and specialized instruments used in MIS laminectomy, there is a well-documented learning curve in which a significantly increased number of durotomy, reoperation rate, incorrect level surgeries occurred in the first 30 cases [6]. In addition, procedure length decreased as a function of the chronological case number.

Conclusions

Minimally invasive laminectomy remains an effective technique in treating symptomatic central and lateral recess lumbar stenosis. As with open laminectomy, the ideal patient for this procedure presents with symptoms of neurogenic claudication or lumbar radiculopathy in the absence of back pain, mechanical instability, high-grade spondylolisthesis, or deformity. Benefits include a smaller skin incision, reduced muscle and midline tension band disruption compared to open approaches, earlier mobilization, and reduced hospital stay.

References

1. Weinstein JN, Lurie JD, Tosteson TD, Hanscom B, Tosteson AN, Blood EA, Birkmeyer NJ, Hilibrand AS, Herkowitz H, Cammisa FP, Albert TJ, Emery SE, Lenke LG, Abdu WA, Longley M, Errico TJ, Hu SS. Surgical versus nonsurgical treatment for lumbar degenerative spondylolisthesis. N Engl J Med. 2007;356(22):2257–70. https://doi.org/10.1056/NEJMoa070302

2. Deutsche Gesellschaft für Neurochirurgie. In: Wüllenweber R, editor. Lumbar disc; adult hydrocephalus: proceedings of the 27th annual meeting of the Deutsche Gesellschaft für Neurochirurgie, Berlin, September 12–15, 1976, Advances in neurosurgery, vol. 4. Berlin: Springer; 1977.

3. Podichetty VK, Spears J, Isaacs RE, Booher J, Biscup RS. Complications associated with minimally invasive decompression for lumbar spinal stenosis. J Spinal Disord Tech. 2006;19(3):161–6. https://doi.org/10.1097/01.bsd.0000188663.46391.73

4. Phan K, Mobbs RJ. Minimally invasive versus open laminectomy for lumbar stenosis: a systematic review and meta-analysis. Spine. 2016;41(2):E91–E100. https://doi.org/10.1097/brs.0000000000001161

5. Palmer S, Turner R, Palmer R. Bilateral decompression of lumbar spinal stenosis involving a unilateral approach with microscope and tubular retractor system. J Neurosurg. 2002;97(2 Suppl):213–7.

6. Sclafani JA, Kim CW. Complications associated with the initial learning curve of minimally invasive spine surgery: a systematic review. Clin Orthop Relat Res. 2014;472(6):1711–7. https://doi.org/10.1007/s11999-014-3495-z

Surgical Embolectomy for Acute Ischemic Stroke

Jaechan Park

This chapter focuses on the role of a surgical embolectomy in the multidisciplinary management of an acute ischemic stroke, especially in cases of occlusion of the internal carotid artery (ICA) or middle cerebral artery (MCA). When endovascular recanalization therapy fails, a surgical embolectomy may be an efficient rescue treatment if the patient is still within the therapeutic time window for restoring the cerebral blood flow. This surgical option is based on the author's clinical experience. A minimally invasive and rapid surgical embolectomy (MIRSE) using a superciliary or supraorbital keyhole approach is a direct and straightforward approach that provides rapid access to the circle of Willis and the occluded vascular lesion. Advancements in surgical techniques to reduce the operative time, effective recanalization of the occluded vessels, and positive surgical results are all presented.

Background

Surgical Embolectomy Revisited

Since 1956, a variety of case reports and small case series have confirmed the effectiveness of a surgical embolectomy for treating an acute middle cerebral artery (MCA) occlusion [1–5]. Conventionally, a surgical embolectomy involves a pterional craniotomy, dissection of the sylvian fissure, a longitudinal incision of the occluded MCA, removal of the embolus via an arteriotomy, and microsuturing to close the arteriotomy.

However, the extended operative time of a surgical embolectomy precludes its use for acute stroke management that has a relatively short therapeutic time window for restoring the cerebral blood flow. Consequently, intravenous (IV) thrombolysis and endovascular recanalization are currently the standard therapies for acute stroke management [6–22].

Following an acute ischemic stroke, the therapeutic time window for restoring the cerebral blood flow differs according to the treatment modality. In the case of intravenous and intra-arterial (IA) thrombolysis, the time window is restricted to 4.5 h and 6 h, respectively [10, 14, 17]; however, an

J. Park, MD, PhD
Department of Neurosurgery, Research Center for Neurosurgical Robotic Systems, Kyungpook National University, 50, Samduk 2-Ga, Jung-Gu, Daegu 700-721, Republic of Korea
e-mail: jparkmd@hotmail.com; jparkneurosurgery@gmail.com

IA mechanical thrombectomy has lengthened the time window to 8 h, according to the Mechanical Embolus Removal in Cerebral Ischemia (MERCI) trial in 2005 that evaluated the safety and efficacy of an endovascular device for restoring the patency of occluded intracranial vessels [21, 22]. Accordingly, the results of endovascular recanalization, along with the extended therapeutic time window and efficacy of recanalization, present a new opportunity for considering the role and efficacy of surgical recanalization. As a result, the present authors utilized the extended 8-h time window from an IA mechanical thrombectomy for performing a surgical embolectomy.

Results of Endovascular Recanalization Therapies

An IA mechanical thrombectomy using recent endovascular devices has achieved high recanalization rates in association with good neurological outcomes and becomes a standard therapy for acute occlusion of proximal intracranial arteries [18–22]. However, despite the application of recent endovascular treatments, including catheter-based devices, stent-based devices, and an IA recombinant tissue plasminogen activator (rt-PA), cases of failed endovascular recanalization still remain.

SOLITAIRE™ with the intention for thrombectomy (SWIFT) trial published in 2012 reported a 69% successful recanalization rate with a grade 2 or 3 thrombolysis in myocardial ischemia (TIMI) flow after using Solitaire [20]. This rate increased to 89% after rescue treatment using other endovascular devices and intra-arterial fibrinolysis.

Meanwhile, in the TREVO 2 trial, also published in 2012, that compared the efficacy and safety of a mechanical thrombectomy using a Trevo Retriever or a Merci Retriever, the Merci group achieved a 66% successful recanalization rate, which increased to 77% after rescue endovascular treatment, while the Trevo group achieved an 85% successful recanalization rate, which increased to 92% after rescue endovascular treatment [18]. Importantly, even following rescue treatment with all available neurovascular thrombectomy devices and IA rt-PA, the recanalization failure rate was still 11% and 8% in the SWIFT and TREVO 2 trial, respectively. Thus, surgical treatment can offer an important rescue solution in the case of endovascular failure when the time after stroke symptom onset is still within 8 h.

Interdisciplinary Management for Acute Ischemic Stroke

Overall Strategy

Maximizing the successful recanalization rate requires coordinated interdisciplinary management of all available tools, including the medical, endovascular, and surgical methods. At the author's institution, the departments of emergency medicine, cardiology, radiology, neurology, and neurosurgery are all connected with the national cardiocerebrovascular center.

For ischemic stroke patients, intravenous (IV) thrombolysis is initiated within 4.5 h after symptom onset. If the initial CTA or MRA shows a large proximal vessel occlusion, the patient is immediately moved to the angiography suite.

In the case of IV rt-PA failure or contraindication, an IA mechanical thrombectomy is attempted based on the following inclusion criteria: (1) the occlusion of a large proximal vessel, (2) the patient is within 8 h after stroke onset, and (3) a significant MRI diffusion-weighted imaging (DWI)/perfusion-weighted imaging (PWI) mismatch. If all of the available endovascular devices and IA rt-PA are unsuccessful, an immediate surgical rescue treatment is attempted. In the case of endovascular failure, some patients can still undergo a surgical embolectomy, as long as they are still within the therapeutic time window.

Indications of Surgical Embolectomy

A surgical embolectomy can be considered based on the following inclusion criteria. First, the therapeutic time window for surgical recanalization is up to 8 h after symptom onset [23, 24]. This is essentially the therapeutic time window for endovascular mechanical recanalization, as there has been no multicenter, randomized, prospective clinical trial for surgical embolectomies.

Notwithstanding, according to the criteria proposed by Dávalos *et al.* [25], patients with a clinical/DWI mismatch, defined as a DWI lesion volume less than 25 mL and National Institutes of Health Stroke Scale (NIHSS) score of 8 or greater, can have an extended therapeutic time window. While the DWI lesion may become enlarged, there is good leptomeningeal collateralization to extend the therapeutic time window.

Second, a significant DWI/PWI mismatch in the MRI is critical. Thus, after the failure of endovascular recanalization therapy, if immediate MR imaging is possible, a repeated DWI is recommended to exclude cases of rapid conversion to a matched DWI/PWI pattern.

Third, the occlusion is in the supraclinoid ICA, M1, or proximal M2 segment of the MCA or the A1 or proximal A2 segment of the ACA. Most commonly, the surgical target is an occlusion in the supraclinoid ICA and/or M1 segment including the MCA bifurcation area.

Fourth, an embolic occlusion is more suitable than an in situ thrombosis, where the former can be predicted based on the associated cardiac arrhythmia, angiographic findings, and the response of the clot to the endovascular procedures.

Presurgical Steps

Presurgical Procedures

The presurgical steps are all performed as rapidly as possible, including a repeated DWI, the acquisition of informed consent, transport to the operating room, and the induction of general anesthesia. Furthermore, since a surgical embolectomy does not require a central venous line, the presurgical steps from the declaration of endovascular failure to the skin incision can take less than 1 h.

The major limitation of this surgical strategy is the time required for patient preparation and transport to the operating room; however, this can be effectively shortened with the use of a hybrid neurovascular facility combining an angiography suite and operating room [26–28].

Surgical Informed Consent

Obtaining surgical informed consent necessitates appropriate information being given to the patient's family by the physicians involved in the surgical procedure, including the patient's condition, the prognosis without recanalization, and the attendant risks and benefits of a surgical embolectomy as the recommended treatment.

For the purpose of comparison, where the outcomes for recanalized patients who undergo a surgical embolectomy can be considered as similar to the outcomes for revascularized patients who undergo endovascular mechanical recanalization therapy, the results of the Multi MERCI trial published in 2008 reported that 49%, 26%, and 25% of the revascularized patients who underwent endovascular mechanical recanalization therapy achieved mRS ≤2, 3–5, and 6, respectively, while 10%, 38%, and 52% of the non-revascularized patients achieved mRS ≤2, 3–5, and 6, respectively [21].

Surgical Techniques

Craniotomies

A pterional craniotomy or variant is commonly used for patients with an ICA and/or MCA occlusion, as it provides wide access to occlusion sites in the supraclinoid ICA, M1, M2, M3, and M4 segments of the MCA [1–5]. Notwithstanding, since most occlusions involve the ICA, M1 segment, or MCA division, smaller craniotomies are invariably adequate to access the lesions [23, 24].

The options for a minimally invasive surgical technique include a pterional mini-craniotomy and supraorbital mini-craniotomy, and the surgeon needs to choose the most appropriate to reduce the operative time.

Embolectomy

The dural incision is performed using an operating microscope, and the carotid cistern is then opened to achieve brain relaxation and frontal lobe retraction. Proximal opening of the sylvian fissure permits visualization up to the carotid bifurcation without temporal lobe traction, and further dissection of the distal sylvian fissure exposes the M1 and proximal M2 segments of the MCA.

Normally, the occluded segment of the vessel due to an intravascular blood clot appears bluish, firm, and expanded (Fig. 1); however, occasionally, the occluded vessel can appear white with no expansion in a case of a small, white-colored embolus that is mainly composed of platelets.

A proximal temporary clip is applied to the occlusion, and a longitudinal incision is then made in the superior wall of the occluded segment of the vessel that does not exhibit any atherosclerotic change. A 3-mm arteriotomy is usually enough to remove the intravascular blood clot
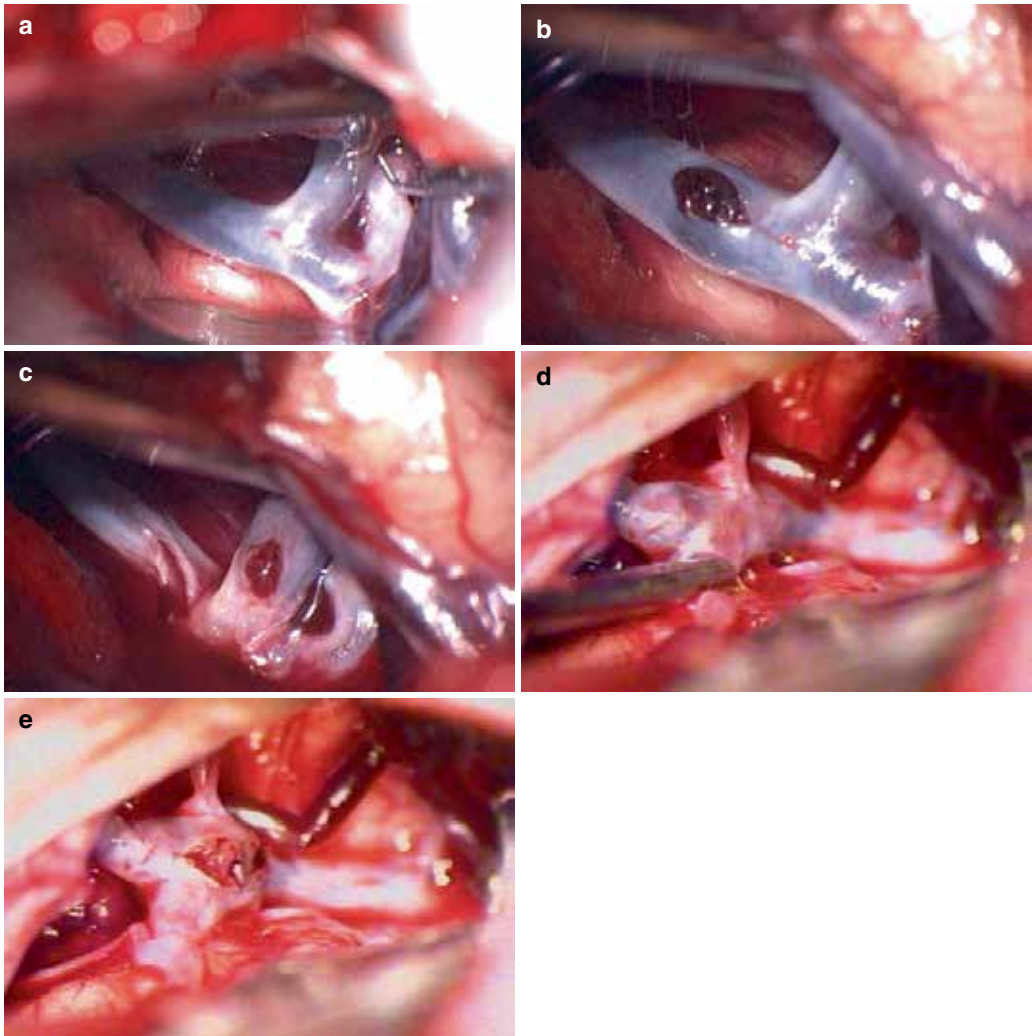
Fig. 1: Intraoperative photographs showing embolic occlusion of the intracranial arteries. In Case 1, the occluded segment of the MCA is *bluish* and firm (**a–c**), whereas in Case 2, the occluded segment of the ICA (**d, e**) is *bluish*, firm, and expanded.

and also easy to repair. According to the location and number of emboli, one to three arteriotomies are normally sufficient.

A solid embolus is extracted via the arteriotomy using forceps, while a viscous clot proximal to a solid embolus can be removed in several ways, including opening the proximal temporary clip to allow an antegrade flow, suction through the arteriotomy, or sequential compression (squeezing) of the artery using forceps. After verifying the antegrade blood flow through a proximal artery, the retrograde blood flow needs to be ascertained. In the case of no retrograde flow, suction

through the arteriotomy, sequential compression of the distal artery, and then another arteriotomy may be required.

Repair of Arteriotomy

The last step before reperfusion is repairing the arteriotomy, which can be performed using three surgical techniques. The first option is a conventional microsuture technique [1–5], which involves temporarily trapping the arteriotomy site and 8–0 monofilament sutures to close an arteriotomy in the ICA and 9–0 or 10–0 monofilament sutures to close an arteriotomy in the M1segment or a MCA division. This microsuturing technique requires the most time. For the second option, the arteriotomy is simply repaired using a curved or angled aneurysm clip [23, 24]. This is possible when the arteriotomy is <3 mm (Fig. 2a). The clip is applied tangential to the arteriotomy, thereby replacing the microsutures and reducing the operative time. While a standard aneurysm clip can be used to close an arteriotomy in the ICA, a miniclip can be used for an arteriotomy in the MCA. Finally, the third option is applicable when the arteriotomy is >3 mm and cannot be repaired using a tangential clip. This special technique allows immediate cerebral reperfusion as one or two aneurysm clips with curved blades are used as temporary compartmentalizing clips to encircle
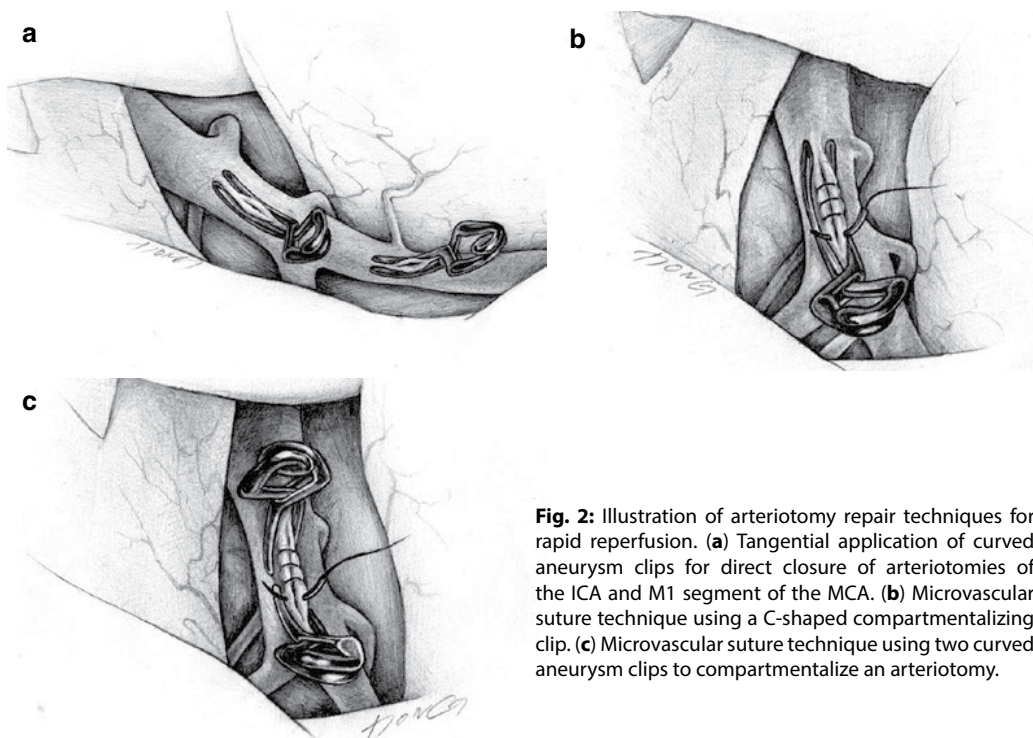
Fig. 2: Illustration of arteriotomy repair techniques for rapid reperfusion. (**a**) Tangential application of curved aneurysm clips for direct closure of arteriotomies of the ICA and M1 segment of the MCA. (**b**) Microvascular suture technique using a C-shaped compartmentalizing clip. (**c**) Microvascular suture technique using two curved aneurysm clips to compartmentalize an arteriotomy.

and separate the arteriotomy site (Fig. 2b, c). This creates a transient vascular conduit below the clip blades, allowing a cerebral blood flow during microsuturing. The clips are then removed after the repair is finished [29].

Minimally Invasive and Rapid Surgical Embolectomy (MIRSE)

The lengthy surgical procedures involved in a conventional surgical embolectomy are unsuitable for endovascular techniques in the case of an acute ischemic stroke [1–5]. In contrast, the recently developed MIRSE technique enables rapid surgical recanalization in a minimally invasive manner within a limited therapeutic time window [23, 24]. Reflecting the acute ischemic stroke management concept of "time is brain," MIRSE minimizes both the surgical invasiveness and the operative time for cerebral reperfusion.

Undoubtedly, the limitations of minimally invasive surgery with a small cranial opening include narrow viewing angles, reduced intraoperative light, reduced maneuverability of the microinstruments, and unidirectional application and coaxial control of the instruments. Yet, these limitations can be overcome using specialized surgical techniques and with surgical experience. Thus, the MIRSE technique consists of a superciliary keyhole approach, an arteriotomy for removing the embolus, and arteriotomy repair techniques for obtaining rapid reperfusion in the case of a small limited craniotomy.

A keyhole approach has several advantages, including rapid access to the lesion with a small operative wound, reduced wound-related pain, no intraoperative blood transfusion, minimal occurrence of postoperative epidural hematomas, an early return to work and normal life, and a decreased patient reluctance for surgery.

Superciliary Keyhole Approach

The MIRSE procedure begins with a superciliary keyhole approach, consisting of a 4-cm eyebrow incision starting from the midpupillary line and a supraorbital mini-craniotomy (Fig. 3) [23, 24]. This superciliary keyhole approach has already been used for tumorous and vascular lesions of the anterior cranial fossa and parasellar region [30–37]. While the surgical embolectomy procedures require a 4-cm or 4.5-cm eyebrow incision, unruptured aneurysms can be clipped using just a 3.5-cm eyebrow incision.

Despite the small superciliary skin incision, a relatively large craniotomy is created by cutting and splaying the underlying muscles. A high-speed drill with a footplate attachment is then used to drill a frontobasal lateral burr hole and create a supraorbital bone flap with a diameter of >2 cm. Before drilling, unidirectional skin retraction using a retractor held by an assistant can avoid skin damage and create sufficient space for the craniotomy. Six retraction sutures are positioned at the edge of the skin incision. The inner edge of the craniotomy above the orbital rim is drilled and beveled, while the frontal floor prominences are flattened. Plus, to expose the sylvian fissure area, the sphenoid ridge adjacent to the frontobasal lateral burrhole is slightly drilled.

Table 1: Summary of patients who underwent a MIRSE after the failure of endovascular recanalization for acute ischemic stroke.

Case no.	1	2	3	4	5	6	7	8	9	10
Age (year)/sex	50/M	42/F	68/M	28/M	56/M	50/F	69/F	78/F	39/F	71/F
Occluded vessel	Rt MCA	Lt MCA	Lt ICA/MCA	Rt ICA/MCA	Lt ICA	Rt MCA	Rt ICA	Rt ICA	Rt ICA	Lt MCA
Cause of stroke	Cardiogenic	Cardiogenic	Cardiogenic	Carotid dissection	Ruptured aneurysm coiling	ICA web	Cardiogenic	Cardiogenic	Cardiogenic	Cardiogenic
Initial NIHSS after stroke	11	15	16	12	15	13	19	18	11	15
Time interval (h)										
Symptom to endovascular failure	4.5	6.0	6.0	5.5	1.2	3.5	3.2	6.0	3.0	4.0
Skin incision to reperfusion	1.0	1.5	1.5	1.0	0.9	0.7	0.7	0.8	0.8	0.8
Symptom onset to reperfusion	7.0	8.5	8.5	7.5	3.0	5.2	4.7	7.6	4.5	6.0
Arteriotomy repair	Aneurysm clip	9–0 sutures, clip	9–0 sutures, clip	Aneurysm clip	8–0 sutures	Aneurysm clip	Aneurysm clip	8–0 sutures	8–0 sutures	9–0 sutures
Postop TICI	3	3	3	2	3	3	3	3	3	3
NIHSS, 7 days	3	6	Dead	8	6	6	8	12	8	4
mRS, 3 months	0	1	Dead	3	1	1	2	3	1	1

ICA internal carotid artery, *MCA* middle cerebral artery, *mRS* modified Rankin scale, *NIHSS* National Institute of Health Stroke Scale, *TICI* thrombolysis in cerebral infarction
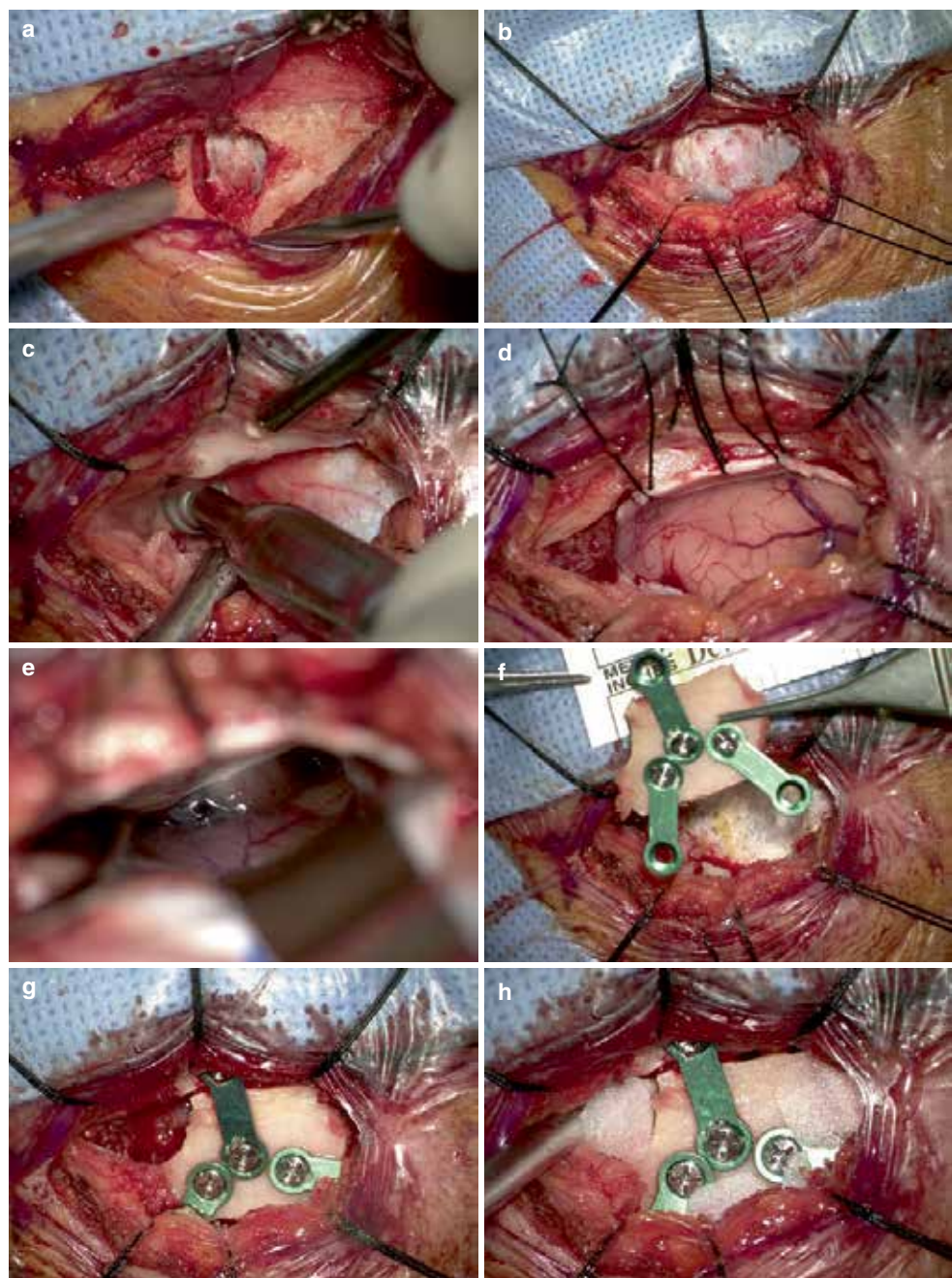
Fig. 3: Operative photographs showing the procedures of a superciliary keyhole approach. (**a**) Drilling of key burrhole. (**b**) Six stay sutures with mosquito clamps after creating a bone flap. (**c**) Lateral extension of craniotomy by drilling the sphenoid ridge. (**d**) C-shaped dural incision. (**e**) Opening an optic nerve cistern through a small cranial opening. (**f**) Small bone flap with attached plates. (**g**) Bone flap in place. (**h**) Key burrhole and bone gaps covered with porous high-density polyethylene implants. (**i**) Pericranial sutures. (**j**) Muscular sutures.

(Cont'd.)...
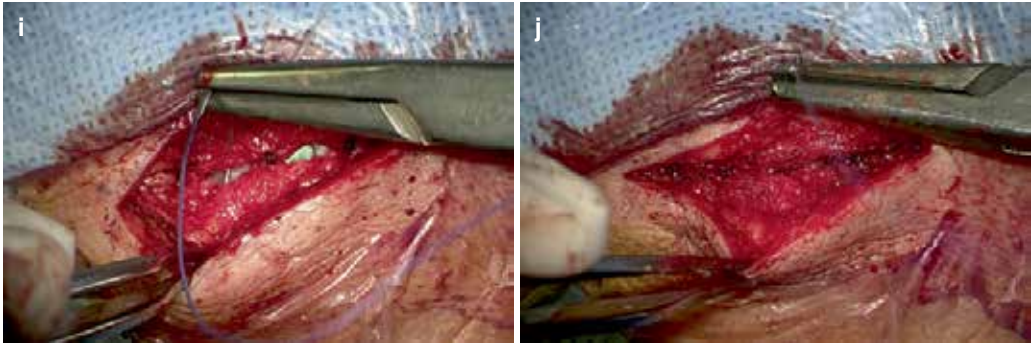
Fig. 3: *...(Cont'd.)*

Intradural Procedures

Following the dural incision, an operating microscope is used to slide a narrow brain spatula over the base of the frontal lobe toward the carotid and optic nerve cisterns, which are then opened to drain the cerebrospinal fluid, achieve brain relaxation, and obtain an intracranial working space. To expose the supraclinoid ICA, dissecting the proximal sylvian fissure provides more frontal lobe retraction and visualization up to the carotid bifurcation. Additional dissection of the sylvian fissure exposes the M1 segment, MCA bifurcation at the MCA genu, and proximal M2 segment. As the sylvian dissection is performed along the frontal side of the sylvian veins, the division of some small fronto-sylvian veins is inevitable.

The identification of the occluded vessel segment, arteriotomy, intravascular blood clot removal, and verification of the antegrade and retrograde blood flow by opening the temporary clips proximal and distal to the arteriotomy are all performed as described above. All these tasks can be effectively performed via a keyhole approach.

Repairing the arteriotomy is the last step before cerebral reperfusion. Among the three above-mentioned techniques for repairing the arteriotomy, microsuturing is the most challenging via a keyhole approach. While passing a needle through the vascular wall in a running manner is feasible using a right-hand needleholder, tying a knot, which involves four separate actions (picking up the thread with the left-hand forceps, making a loop around the tip of the right-hand forceps, picking up the short end of the thread with the right-hand forceps, and pulling the loop off the right-hand forceps), can be difficult when using microinstruments with coaxial movement through a small cranial opening.

Therefore, a new clip-knotting technique is used for tying a knot after microsuturing via a keyhole approach (Fig. 4) [38]. With the needleholder in the right hand, the needle and a short (5 cm) thread are passed through the vessel wall several times in a running manner along the arterial incision. After tightening the running stitch to approximate the edges of the lesion, the ends of the thread are both held with forceps using the left hand. To hold both threads in place, an aneurysm clip is then applied using a right-hand clip applier, and any remaining thread beyond the clip is cut appropriately.
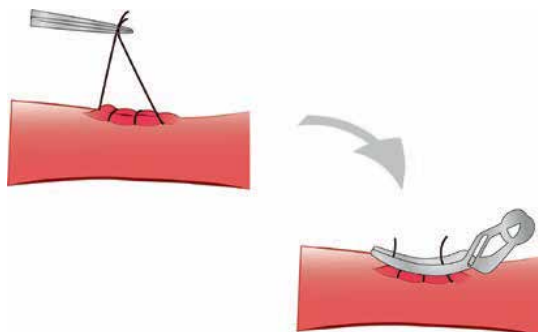
Fig. 4: Clip-knotting technique for repairing an artery via a keyhole approach. After pulling the running stitch tight to approximate the edges of the arteriotomy, both threads are held in place using an aneurysm clip.

If the arterial incision is <3 mm, the simplest way to repair the arteriotomy is the tangential application of a curved or angled aneurysm clip [23, 24].

Postoperative Course

Surgical Results

Our clinical experience has shown that a MIRSE procedure is effective for recanalizing an occluded ICA and MCA in patients with an acute ischemic stroke, as the high recanalization rate and short operative time can provide a final rescue treatment following the failure of endovascular recanalization.

Table 1 presents the characteristics of the patients who underwent a MIRSE for an acute occlusion of the MCA and ICA ($n = 2$), MCA ($n = 4$), and ICA ($n = 4$). Reperfusion with the MIRSE was accomplished within 3.0–8.5 h after symptom onset. Complete recanalization was achieved in all ten patients.

At 3 months, nine of the recanalized patients showed mRS grades of 0 ($n = 1$), 1 ($n = 5$), 2 ($n = 1$), and 3 ($n = 2$). One patient (Patient No. 3) developed a fatal hemorrhage in the basal ganglia several hours after recanalization.

Subdural Fluid Collection

Surgical dissection of the basal cisterns and sylvian fissure, as performed during aneurysm surgery and a surgical embolectomy, is sometimes followed by the postoperative occurrence of a subdural hygroma and resultant chronic subdural hematoma (CSDH).

The sequence behind the occurrence of a subdural hygroma is most probably as follows: after surgical dissection of the arachnoid membrane, a one-way valve is formed due to adhesion of the arachnoid during the healing process, and CSF is then accumulated in the subdural space via this one-way valve [39, 40]. Meanwhile, tearing of the stretched bridging veins and bleeding from the neomembrane of a CSDH may also contribute to development and enlargement of a CSDH.

Although the exact incidence and risk factors of a subdural hygroma and CSDH following a surgical embolectomy are not known, they can be estimated based on previous studies of

unruptured intracranial aneurysms, where an advanced age and male gender were identified as risk factors for a CSDH following unruptured aneurysm surgery [41–45].

Intracranial Hemorrhage

In the MERCI and Multi MERCI trials, 7.8% and 9.8% of the patients who underwent endovascular mechanical recanalization therapy developed symptomatic intracranial hemorrhages, subarachnoid or intraparenchymal, respectively [21, 22].

An intracranial hemorrhage can also occur after a surgical embolectomy and recanalization. One of our ten MIRSE patients (Case No. 3) developed a fatal intracerebral hemorrhage in the basal ganglia following successful recanalization [23].

Frontalis Muscle Palsy

The risk of frontalis muscle palsy due to an injury of the frontal branch of the facial nerve can also be a concern with a superciliary keyhole approach. However, none of the MIRSE patients developed permanent palsy of the frontalis muscle, plus our previous case series of unruptured aneurysms had a negligible incidence (<1%) of permanent palsy of the frontalis muscle, although transient severe palsy occurred in approximately 20% of the patients [46].

Case Illustrations

Case No. 6

A 50-year-old woman presented with left hemiplegia for 1 h. As no intracranial hemorrhage was revealed on a CT scan, intravenous rt-PA was administered immediately. Diffusion-weighted imaging showed faint hyperintensities in the right temporal lobe and paraventricular region, while the perfusion defect on the time-to-peak (TTP) maps involved the entire right MCA territory. Carotid angiograms showed a distal occlusion of the right M1 segment of the MCA (Fig. 5a) and a linear filling defect corresponding to a carotid web at the right internal carotid origin (Fig. 5b). While endovascular recanalization therapy was successful in an inferior division of the right MCA, a Penumbra reperfusion catheter and Solitaire AB stent were both unsuccessful in recanalizing the superior division of the MCA (Fig. 5c).

Following the endovascular failure, the MIRSE presurgical steps took 1 h, including a repeated DWI, informed consent from the patient's family, transport to the operating room, and the induction of general anesthesia. A supraorbital mini-craniotomy revealed an embolic occlusion in the superior division of the MCA, which appeared as a bluish expanded segment (Fig. 5d–e). A small 3-mm arteriotomy in the occluded segment allowed the embolus to be removed, and an aneurysm miniclip with a curved blade was used to repair the arteriotomy (Fig. 5f–g). Reperfusion was achieved 40 min after the skin incision and 5.2 h after symptom onset.
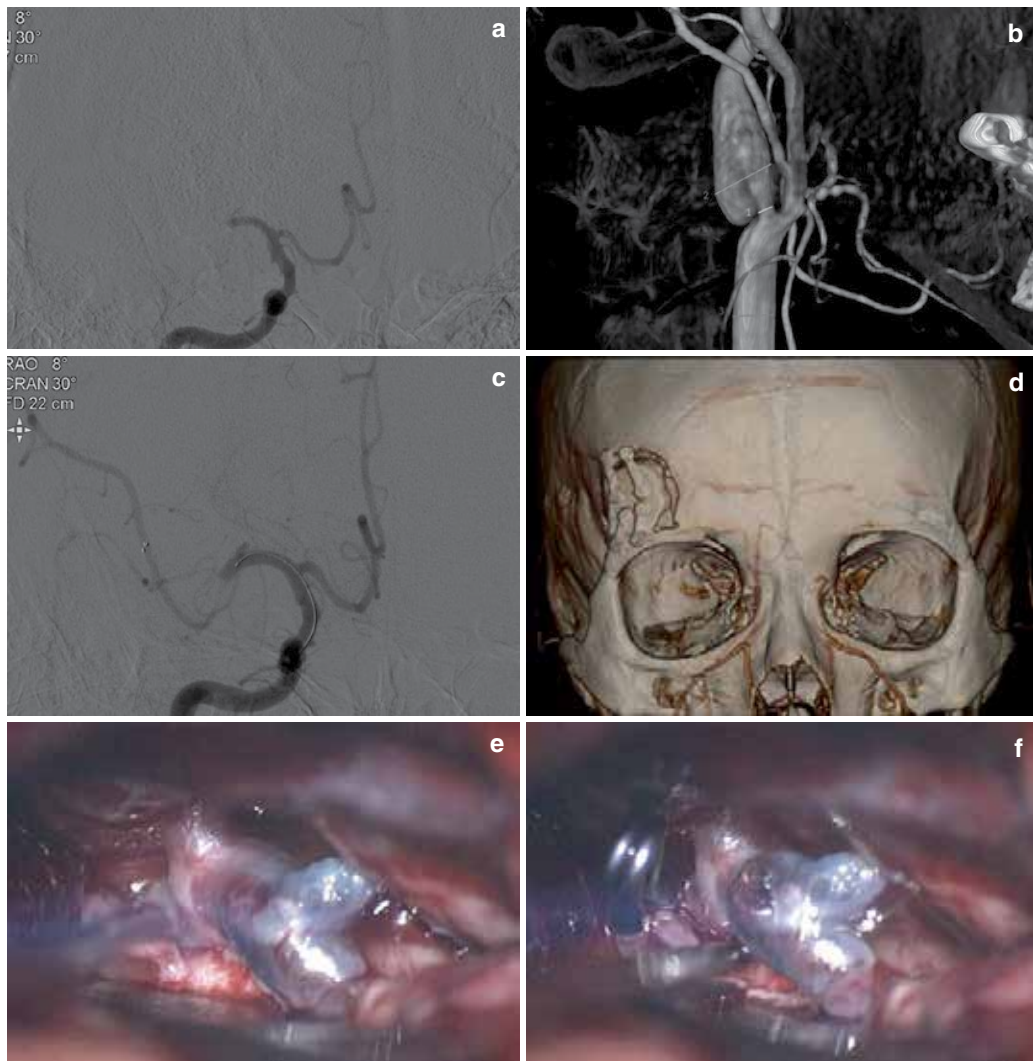
Fig. 5: Illustrative Case 6. (**a**) Initial carotid angiogram revealing an occlusion of the distal M1 segment of the right MCA. (**b**) Carotid angiogram demonstrating a carotid web at the right internal carotid origin. (**c**) Carotid angiogram demonstrating an occlusion of the superior division of the MCA following endovascular recanalization procedures. (**d**) Postoperative CT showing supraorbital mini-craniotomy. (**e**) Intraoperative photograph showing an embolic occlusion of the superior division of the MCA, revealed as a bluish and expanded segment. (**f**) Intraoperative photograph showing the occluded vessel with arteriotomy. (**g**) Intraoperative photograph showing the recanalized MCA after repair of the arteriotomy using an aneurysm clip. (**h**) Postoperative carotid angiogram showing complete restoration of flow in the occluded MCA. (**i–l**) Intraoperative photographs showing surgery resecting the carotid web.

(Cont'd.)...
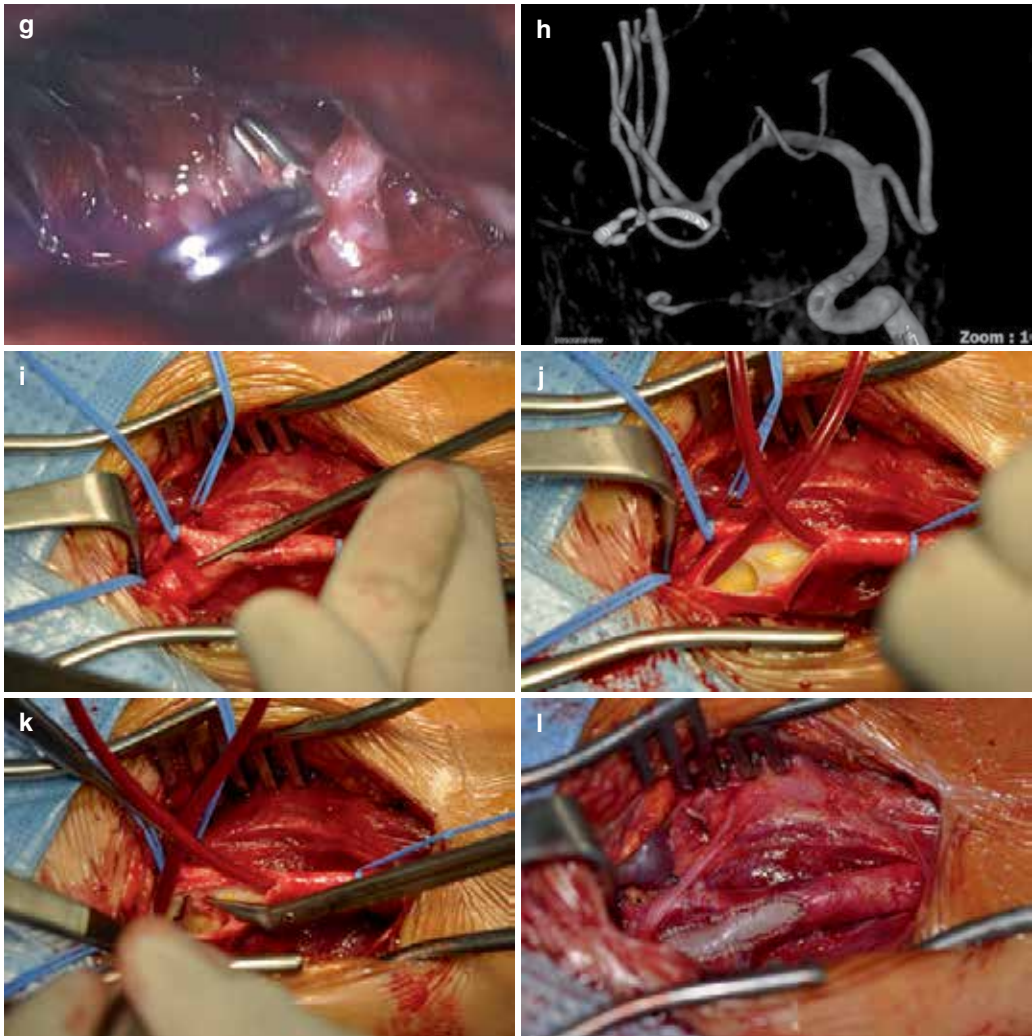
Fig. 5: *...(Cont'd.)*

Postoperative day 1 showed a significant improvement in the patient's hemiplegia (grade 3.5), and an angiogram confirmed complete restoration of flow in the occluded MCA (Fig. 5h). At 3 months, the only sequel was a slight weakness of the left hand, while the cosmetic results of the operative wound were excellent. At 1 year, the patient underwent surgical resection of the carotid web (Fig. 5i–l), allowing a change from anticoagulant to antiplatelet medication.

After taking 1 h for the angiography and endovascular recanalization procedure, repeated DWI was used to check for any significant increase in the lesion size, and then the patient was immediately rushed to the operating room. Thus, it only took 50 min from the declaration of endovascular failure to the induction of general anesthesia in the operating room.
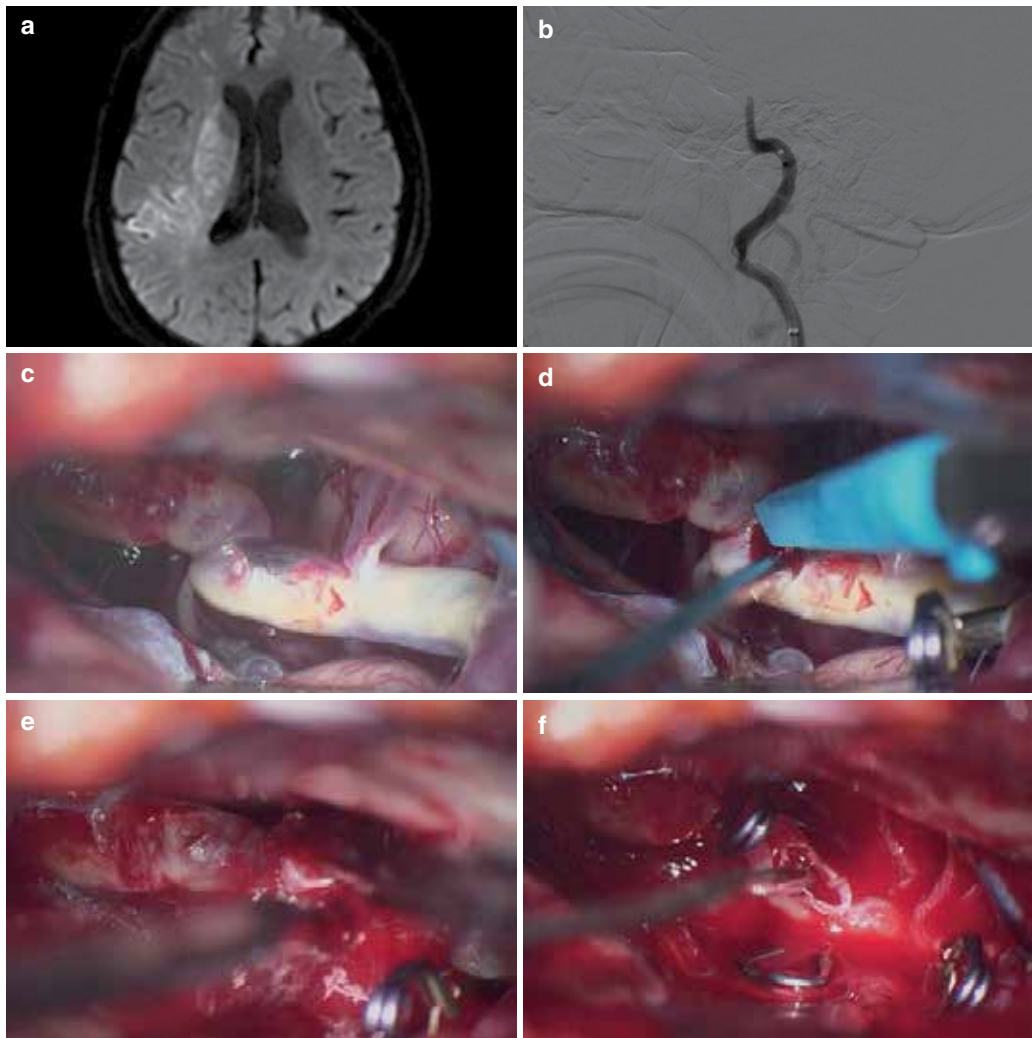
Fig. 6: Illustrative Case 8. (**a**) Initial DWI showing hyperintensity in the right paraventricular area. (**b**) Initial carotid angiogram revealing an occlusion of the right ICA. (**c**) Intraoperative photograph showing the supraclinoid ICA that was severely atherosclerotic. (**d–f**) Intraoperative photographs showing the removal of the accidently detached Solitaire stent through an arteriotomy in the ICA. (**g**) Intraoperative photograph showing the repair of the arteriotomy using microsutures after applying a compartmentalizing clip. (**h**) Sutured arteriotomy reinforced with a permanent aneurysm clip. (**i**) Postoperative carotid angiogram showing complete restoration of the blood flow.

(Cont'd.)...
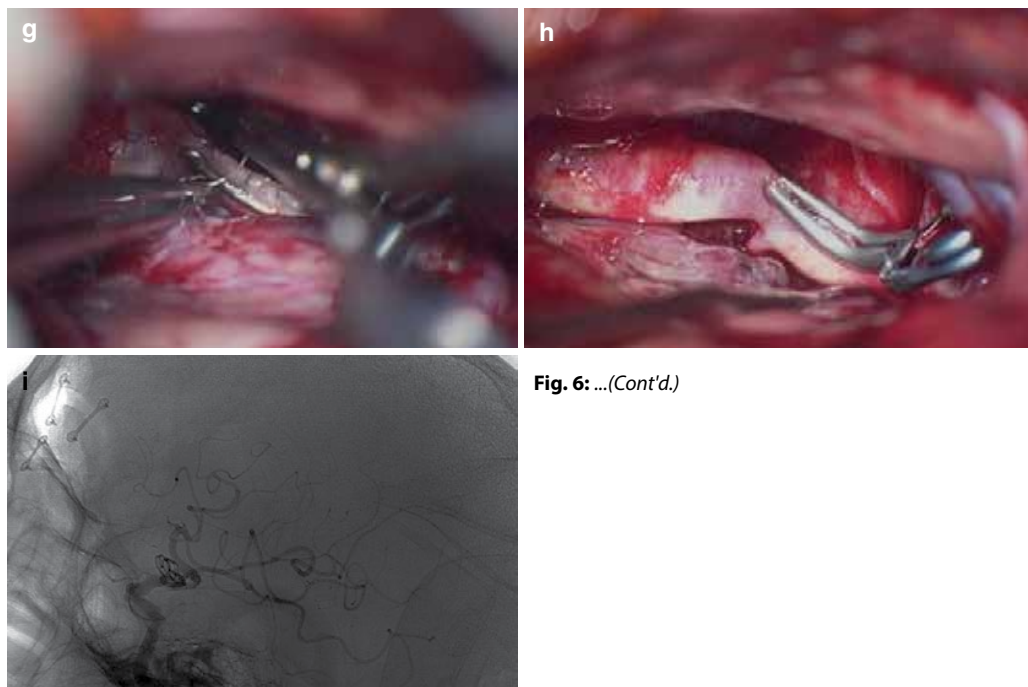
Fig. 6: *...(Cont'd.)*

The supraorbital keyhole approach included a 4-cm eyebrow incision and supraorbital mini-craniotomy. After opening the carotid cistern and proximal sylvian fissure, the intracranial ICA was revealed as severely atherosclerotic and occluded with the Solitaire stent harboring the embolus (Fig. 6c). A 5-mm longitudinal incision was made in the superior wall of the ICA containing the distal end of the stent, and then the stent and the associated embolus were extracted using fine forceps (Fig. 6d–f). Next, a compartmentalizing clip with C-shaped blades was temporarily applied to the ICA encompassing the arteriotomy, which was then repaired using 8–0 monofilament polypropylene sutures through the small cranial opening (Fig. 6g–h). Thus, the compartmentalizing clip allowed immediate blood flow during the final repair of the arteriotomy. Only 35 min elapsed from the skin incision to cerebral reperfusion via the vascular conduit below the clip, thereby valuing the concept of "time is brain."

Complete recanalization of the ICA was revealed by postoperative angiography (Fig. 6i), and the perfusion defect in the time-to-peak maps was normalized. At 3 months after surgery, the patient's neurological deficits had improved and her NIHSS score was 8.

Case No. 10

A 71-year-old woman presented with acute onset of right hemiplegia and aphasia. DWI revealed hyperintensities in the left putaminal area and paraventricular region (Fig. 7a), while the perfusion defect on the TTP maps involved the entire left MCA territory (Fig. 7b). Carotid angiograms showed an occlusion of the left M1 segment of the MCA (Fig. 7c). Endovascular recanalization
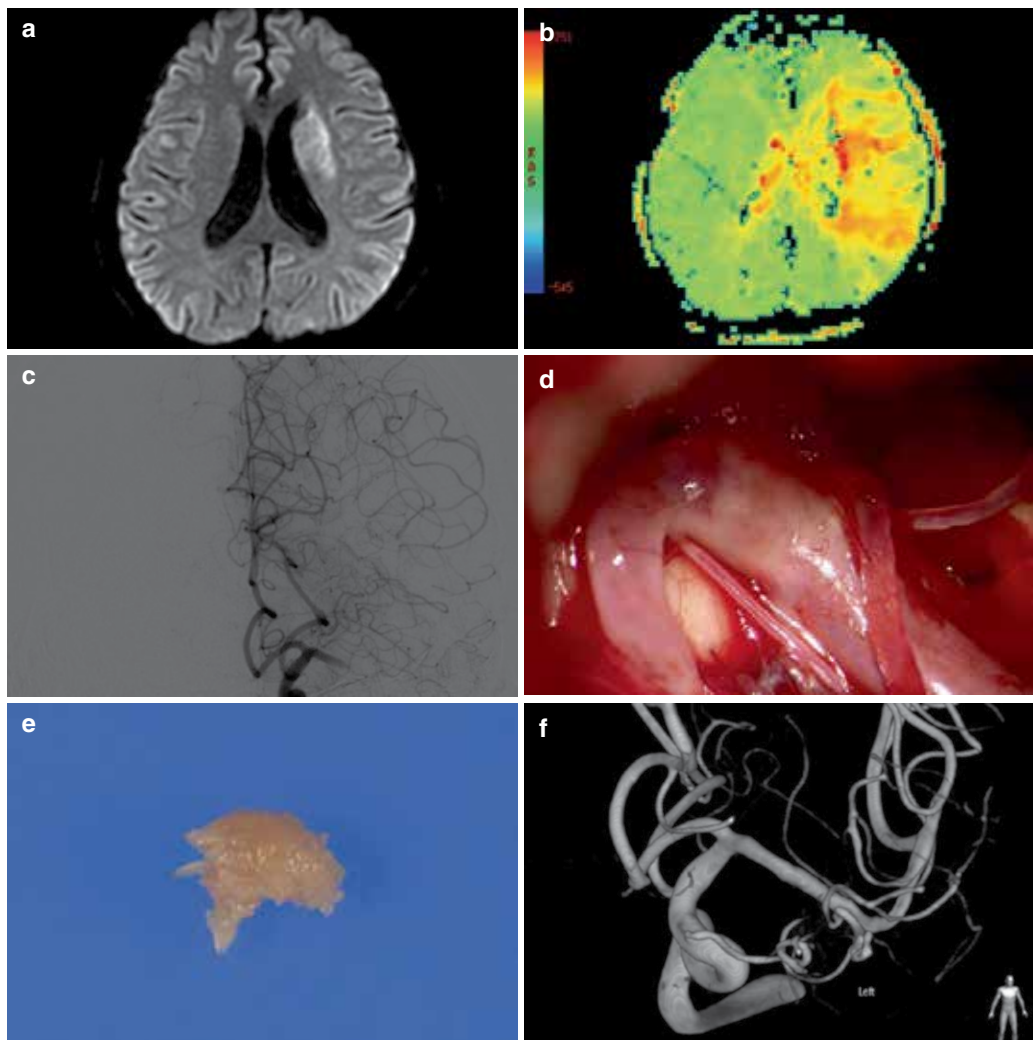
Fig. 7: Illustrative Case 10. (**a**) Initial DWI showing hyperintensity in the right putamen and paraventricular area. (**b**) Perfusion defect on the TTP maps involving the entire left MCA territory. (**c**) Carotid angiogram showing complete occlusion of the M1 segment of the left MCA. (**d**) Intraoperative photograph revealing a short *white* segment of the M1 segment. (**e**) Small, *white*, and hard embolus removed from the white segment of the MCA. (**f**) Postoperative carotid angiogram showing complete restoration of the blood flow.

therapy was attempted using a Penumbra reperfusion catheter and Solitaire stent, yet without success.

A MIRSE was immediately performed and a superciliary keyhole approach revealed the left M1 segment. While there was no bluish and expanded segment suggesting an intravascular blood clot, a whitish segment without expansion was found (Fig. 7d). A white and hard embolus was then revealed via an arteriotomy of the whitish segment (Fig. 7e). The clip-knotting technique was used to repair the arteriotomy after removing the embolus. Reperfusion was achieved 50 min after the skin incision and 6 h after symptom onset.

Postoperative day 1 showed an improvement in the patient's hemiplegia to grade 3.5, and an angiogram confirmed complete restoration of flow in the occluded MCA (Fig. 7f). At 3 months, the only sequel was a slight clumsiness of the right hand.

References

1. Garrido E, Stein BM. Middle cerebral artery embolectomy. Case report. J Neurosurg. 1976;44:517–21.
2. Horiuchi T, Nitta J, Sakai K, *et al*. Emergency embolectomy for treatment of acute middle cerebral artery occlusion. J Neurosurg. 2007;106:257–62.
3. Linskey ME, Sekhar LN, Hecht ST. Emergency embolectomy for embolic occlusion of the middle cerebral artery after internal carotid artery balloon test occlusion. J Neurosurg. 1992;77:134–8.
4. Meyer FB, Piepgras DG, Sundt Jr TM, *et al*. Emergency embolectomy for acute occlusion of the middle cerebral artery. J Neurosurg. 1985;62:639–47.
5. Welch K. Excision of occlusive lesions of the middle cerebral artery. J Neurosurg. 1956;13:73–80.
6. Brekenfeld C, Schroth G, Mordasini P, *et al*. Impact of retrievable stents on acute ischemic stroke treatment. AJNR Am J Neuroradiol. 2011;32:1269–73.
7. Castaño C, Dorado L, Guerrero C, *et al*. Mechanical thrombectomy with the Solitaire AB device in large artery occlusions of the anterior circulation: a pilot study. Stroke. 2010;41:1836–40.
8. Costalat V, Machi P, Lobotesis K, *et al*. Rescue, combined, and stand-alone thrombectomy in the management of large vessel occlusion stroke using the solitaire device: a prospective 50-patient single-center study: timing, safety, and efficacy. Stroke. 2011;42:1929–35.
9. Gralla J, Brekenfeld C, Mordasini P, *et al*. Mechanical thrombolysis and stenting in acute ischemic stroke. Stroke. 2012;43:280–5.
10. Hacke W, Kaste M, Bluhmki E, ECASS Investigators, *et al*. Thrombolysis with alteplase 3 to 4.5 hours after acute ischemic stroke. N Engl J Med. 2008;359:1317–29.
11. Jankowitz B, Aghaebrahim A, Zirra A, *et al*. Manual aspiration thrombectomy: adjunctive endovascular recanalization technique in acute stroke interventions. Stroke. 2012;43:1408–11.
12. Kang DH, Hwang YH, Kim YS, *et al*. Direct thrombus retrieval using the reperfusion catheter of the penumbra system: forced-suction thrombectomy in acute ischemic stroke. AJNR Am J Neuroradiol. 2011;32:283–7.
13. Kang DH, Kim YW, Hwang YH, *et al*. "Switching strategy" for mechanical thrombectomy of acute large vessel occlusion in the anterior circulation. Stroke. 2013;44:3577–9.
14. Kwiatkowski TG, Libman RB, Frankel M, *et al*. Effects of tissue plasminogen activator for acute ischemic stroke at one year. National Institute of Neurological Disorders and Stroke Recombinant Tissue Plasminogen Activator Stroke Study Group. N Engl J Med. 1999;340:1781–7.
15. Mehta B, Leslie-Mazwi TM, Chandra RV, *et al*. Assessing variability in neurointerventional practice patterns for acute ischemic stroke. J Neurointerv Surg. 2013;5(Suppl 1):i52–7.
16. Miteff F, Faulder KC, Goh AC, *et al*. Mechanical thrombectomy with a self-expanding retrievable intracranial stent (Solitaire AB): experience in 26 patients with acute cerebral artery occlusion. AJNR Am J Neuroradiol. 2011;32:1078–81.
17. National Institute of Neurological Disorders and Stroke rt-PA Stroke Study Group. Tissue plasminogen activator for acute ischemic stroke. N Engl J Med. 1995;333:1581–7.
18. Nogueira RG, Lutsep HL, Gupta R, *et al*.; TREVO 2 Trialists (2012) Trevo versus Merci retrievers for thrombectomy revascularisation of large vessel occlusions in acute ischaemic stroke (TREVO 2): a randomized trial. Lancet 380:1231–40
19. Penumbra Pivotal Stroke Trial Investigators. The penumbra pivotal stroke trial: safety and effectiveness of a new generation of mechanical devices for clot removal in intracranial large vessel occlusive disease. Stroke. 2009;40:2761–8.
20. Saver JL, Jahan R, Levy EI, SWIFT Trialists, *et al*. Solitaire flow restoration device versus the Merci Retriever in patients with acute ischaemic stroke (SWIFT): a randomised, parallel-group, non-inferiority trial. Lancet. 2012;380:1241–9.
21. Smith WS, Sung G, Saver J, Frei D, Grobelny T, Hellinger F, Huddle D, Kidwell C, Koroshetz W, Marks M, Nesbit G, Silverman IE, Multi MERCI Investigators, *et al*. Mechanical thrombectomy for acute ischemic stroke: final results of the Multi MERCI trial. Stroke. 2008;39:1205–12.
22. Smith WS, Sung G, Starkman S, MERCI Trial Investigators, *et al*. Safety and efficacy of mechanical embolectomy in acute ischemic stroke: results of the MERCI trial. Stroke. 2005;36:1432–8.

23. Park J, Hwang YH, Kim Y. Extended superciliary approach for middle cerebral artery embolectomy after unsuccessful endovascular recanalization therapy: technical note. Neurosurgery. 2009;65:E1191–4.

24. Park J, Hwang YH, Huh S, et al. Minimally invasive and rapid surgical embolectomy (MIRSE) as rescue treatment following failed endovascular recanalization for acute ischemic stroke. Acta Neurochir. 2014;156:2041–9.

25. Dávalos A, Blanco M, Pedraza S, et al. The clinical-DWI mismatch: a new diagnostic approach to the brain tissue at risk of infarction. Neurology. 2004;62:2187–92.

26. Kotowski M, Sarrafzadeh A, Schatlo B, et al. Intraoperative angiography reloaded: a new hybrid operating theater for combined endovascular and surgical treatment of cerebral arteriovenous malformations: a pilot study on 25 patients. Acta Neurochir. 2013;155:2071–8.

27. Murayama Y, Irie K, Saguchi T, et al. Robotic digital subtraction angiography systems within the hybrid operating room. Neurosurgery. 2011;68:1427–32.

28. Yamakawa K, Kiyama S, Murayama Y, et al. Incidence and neurological outcomes of aneurysm rupture during interventional neuroradiology procedures in a hybrid operating suite. J Anesth. 2012;26:592–4.

29. Park J. Maintenance of cerebral blood flow during microsuture repair of the superior wall of the intracranial internal carotid artery: technical note. World Neurosurg. 2013;80:436.e1–5.

30. Lan Q, Gong Z, Kang D, et al. Microsurgical experience with keyhole operations on intracranial aneurysms. Surg Neurol. 2006;66(1 Suppl):S2–9.

31. Paladino J, Mrak G, Miklic P, et al. The keyhole concept in aneurysm surgery- a comparative study: keyhole versus standard craniotomy. Minim Invasive Neurosurg. 2005;48:251–8.

32. Paladino J, Pirker N, Stimac D, et al. Eyebrow keyhole approach in vascular neurosurgery. Minim Invasive Neurosurg. 1998;41:200–3.

33. Park J, Kang DH, Chun BY. Superciliary keyhole surgery for unruptured posterior communicating artery aneurysms with oculomotor nerve palsy: maximizing symptomatic resolution and minimizing surgical invasiveness. J Neurosurg. 2011;115:700–6.

34. Park J, Woo H, Kang DH, et al. Superciliary keyhole approach for small unruptured aneurysms in anterior cerebral circulation. Neurosurgery. 2011;68(2 Suppl):300–9.

35. Ramos-Zuniga R, Velazquez H, Barajas MA, et al. Trans-supraorbital approach to supratentorial aneurysms. Neurosurgery. 2002;51:125–31.

36. Reisch R, Perneczky A. Ten-year experience with the supraorbital subfrontal approach through an eyebrow skin incision. Neurosurgery. 2005;57(3 Suppl):242–55.

37. Van Lindert E, Perneczky A, Fries G, et al. The supraorbital keyhole approach to supratentorial aneurysms: concept and technique. Surg Neurol. 1998;49:481–90.

38. Park J. Clip-knotting technique for intracranial arterial suturing through deep and narrow surgical corridors-how I do it. Acta Neurochir. 2015;157:769–71.

39. Lee KS. The pathogenesis and clinical significance of traumatic subdural hygroma. Brain Inj. 1998;12:595–603.

40. Yoshimoto Y, Wakai S, Hamano M. External hydrocephalus after aneurysm surgery: paradoxical response to ventricular shunting. J Neurosurg. 1998;88:485–9.

41. Inamasu J, Watabe T, Ganaha T, et al. Clinical characteristics and risk factors of chronic subdural haematoma associated with clipping of unruptured cerebral aneurysms. J Clin Neurosci. 2013;20:1095–8.

42. Mori K, Maeda M. Risk factors for the occurrence of chronic subdural haematomas after neurosurgical procedures. Acta Neurochir (Wien). 2003;145:533–9.

43. Ohno T, Iihara K, Takahashi JC, et al. Incidence and risk factors of chronic subdural hematoma after aneurysmal clipping. World Neurosurg. 2013;80:534–7.

44. Park J, Cho JH, Goh DH, et al. Postoperative subdural hygroma and chronic subdural hematoma after unruptured aneurysm surgery: age, sex, and aneurysm location as independent risk factors. J Neurosurg. 2016;124:310–7.

45. Tanaka Y, Mizuno M, Kobayashi S, et al. Subdural fluid collection following craniotomy. Surg Neurol. 1987;27:353–6.

46. Park J, Jung TD, Kang DH, et al. Preoperative percutaneous mapping of the frontal branch of the facial nerve to assess the risk of frontalis muscle palsy after a supraorbital keyhole approach. J Neurosurg. 2013;118:1114–9.

Abbott